IMPROVED DROUGHT EARLY WARNING AND FORECASTING TO STRENGTHEN PREPAREDNESS AND ADAPTATION TO DROUGHTS IN AFRICA

DEWFORA

A 7th Framework Programme Collaborative Research Project

Potential to supplementing drought early warning systems with new meteorological information

WP4-D4.3

May 2012

Coordinator: Deltares, The Netherlands

Project website: www.dewfora.net

FP7 Call ENV-2010-1.3.3.1

Contract no. 265454

Page intentionally left blank

DOCUMENT INFORMATION

Title	Potential to supplementing drought early warning systems with new meteorological information
Lead Author	ECMWF : Emanuel Dutra, Fredrik Wetterhall, Francesca Di Giuseppe and Florian Pappenberger
Contributors	
Distribution	PU: Public
Reference	WP4-D4.3

DOCUMENT HISTORY

Date	Revision	Prepared by	Organisation	Approved by	Notes

ACKNOWLEDGEMENT

The research leading to these results has received funding from the European Union's Seventh Framework Programme (FP7/2007-2013) under grant agreement N°265454.

We thank our colleagues at ECMWF Franco Molteni, Roberto Buizza and Dick Dee, and Samuel Fournet from PIK for their support.

Page intentionally left blank

Summary

This study investigates the potential to supplement drought early warning systems with new meteorological information. We develop an integrated monitoring and forecasting system based on the Standard precipitation index (SPI), multiple globally available precipitation products (Era Interim and CAMSOPI), which are available in near real time and the ECMWF Seasonal Forecasting System 4. We investigate the capabilities on five basins on the African continent: the Blue Nile, Limpopo, Upper Niger, Oum er-rbia and the Congo. The comparison of the seasonal forecasting system and the global precipitation products shows that there are significant differences in the quality of the precipitation in individual datasets depending on the individual catchments. They can have weaknesses in timing and magnitude and a general statement regarding the best product cannot be done. All the datasets show a good agreement in the South and North West, while there is a low agreement in Central Africa (between the +/- 20° parallels). This can be also seen in the SPI which not only creates difficulties in defining ground truth but also in choosing an adequate product for the monitoring. Therefore, the usefulness of individual near-real time monitoring tools has to be carefully selected depending on region. Seasonal forecasting in the Blue Nile, Limpopo and Upper Niger show a higher reliability and skill in comparison with the Congo and Oum er-rbia. The skill and reliability depend strongly on the accumulation period and more skill is observed at larger accumulation periods. This skill of course partially originates from the observation time period. We show that the new ECMWF seasonal forecasts (system 4) has predictive skill which is higher than using climatology for most regions. and in regions where no reliable near real-time data is available it is better to use just the seasonal forecast for prediction of droughts.

Page intentionally left blank

TABLE OF CONTENTS

List of figures

LIST of tables

Page intentionally left blank

1. INTRODUCTION

Many parts of Africa rely mainly on the rainy season for livestock and agriculture. Droughts can have a severe impact in these areas which often have a very low resilience and low capabilities to mitigate drought effects. For example, the lack of water management and agricultural infrastructure such as water canalization and irrigation can significantly determine the severity of any event. A sequence of droughts can have huge effects, such as the mega sub-Sahel drought of the 1970s and 80s which claimed thousands of lives. A more recent example is the 2011 drought that afflicted the Horn of Africa (HoA). This two-year drought impacted on more than 10 million people and caused famine, population migration and political instability. Managing the impact of droughts is a key component of increasing resilience. Part of managing any impact is the ability to monitor and forecast the length and geographical extension of droughts. The potential of combining monitoring and forecasting has been widely demonstrated over Africa in other areas such as health, water, energy and agriculture (e.g. Ingram et al. 2002; Jones et al. 2000; Lamb et al. 2011; Millner and Washington 2011; Thomson et al. 2006).

The monitoring component relies on near real time observation of surface variables such as precipitation. These observations can either be derived through the merging of ground observations and remote sensing information or by using re-analysis tools. The forecasting component relies on seasonal forecast. This has increasing potential as the quality of numerical weather predictions over the monthly to seasonal lead-times steadily improves (Simmons and Hollingsworth 2002). One example of such a seasonal forecasting system is the ECMWF seasonal forecasting systems (system-3 and the newly released system-4). Despite the recent model improvements, predicted fields such as temperature, and to a higher extent precipitation, can be biased and in some areas can have little or no skill. This particular the case in Africa, where in-situ observations are scarce and models often show persistent systematic errors. One such example is the prediction of the West Africa monsoon system, where the ECMWF seasonal forecasting system (S4) is able to reproduce the progression of the West Africa monsoon, but has biases in terms of a southerly shift of the precipitation in the main monsoon months of July and August. In other areas of Africa for example in West Africa model skill in predicting summer monsoon rainfall anomalies should mostly benefit from improvements in the ocean analysis since large errors are due to the relevant warm bias in the sea surface temperature over the Gulf of Guinea (Agustí-Panareda et al. 2010; Tompkins and Feudale 2009).

An integrated monitoring and forecasting drought system for four African river basins is designed to explore the current capability of ECMWF products to provide drought information over the Africa continent, This is done by combining globally available precipitation monitoring products with the forecast from S4. The drought is derived from the precipitation

field and defined as an anomaly on the rainfall accumulation over a period of time using the Standardized Precipitation Index (SPI). The five selected basins were chosen as representatives of the different synoptic conditions typical of the African continent, where in-situ discharge measurements were available, and include the four regional case studies of the DEWFORA (www.dewfora.net) project.

2. DATA AND METHODS

2.1 PRECIPITATION DATA

2.1.1 Monitoring

There are multiple technical requirements for a data set so that it can form part of an operational monitoring and forecasting chain.

Firstly, the precipitation datasets used for meteorological drought analysis with the SPI should be long enough (at least 30 years, as recommended by Mckee et al. (1993)) and statistically homogeneous. This means for example that observations should as much as possible (i) avoid changes in rain-gauges location and measuring equipments; (ii) use similar techniques to derive precipitation from remote sensing data, even when using different platforms. When using dynamical models output, the model should have the same spatial and temporal structure (as in reanalysis or global/regional climate models) to avoid disruptions due to model changes, such as a change in resolution or parameterization schemes. Changes in the observation systems and/or models can produce artificial signals, such as trends, that will be reflected in the SPI.

Secondly, the data set needs to be available in near-real time, meaning no more than 1 month delay. The long-term homogeneity and near-real time update are two criteria difficult to achieve using both observations and models, especially on a global scale. In this work, we access two products that partially fulfill the requirements: (i) available globally, (ii) at least 30 years of data, (iii) available in near-real time, and (iv) partially temporally homogeneous. From dynamical models, we use the ECMWF ERA-Interim and from observations the CAMSOPI, that are briefly described below.

ERA-Interim (ERAI) is the latest global atmospheric reanalysis produced by ECMWF. ERAI covers the period from 1 January 1979 onwards, and continues to be extended forward in near-real time. Gridded data products include a large variety of 3-hourly surface parameters, describing weather as well as ocean-wave and land-surface conditions, and 6-hourly upper-air parameters covering the troposphere and stratosphere. Vertical integrals of atmospheric fluxes, various synoptic and daily monthly averages, and other derived fields have also been produced. Berrisford et al. (2009) provides a detailed description of the ERAI product archive. Information about the current status of ERAI production, availability of data online, and near-real time updates of various climate indicators derived from ERAI data, can be found at: http://www.ecmwf.int/research/era . Dee et al. (2011) presents a detailed description of the ERAI model and data assimilation system, the observations used, and various performance aspects. The dynamical core of the atmospheric model is based on a

spectral representation for the basic dynamical variables, a hybrid vertical coordinate, and a semi-Lagrangean semi-implicit time stepping scheme.

The ERAI configuration has a spectral T255 horizontal resolution, which corresponds to approximately 79 km spacing on a reduced Gaussian grid. The vertical resolution has 60 model levels with the top of the atmosphere located at 0.1 hPa. The land surface scheme used is TESSEL (Van den Hurk et al. 2000), the predecessor of HTESSEL (Balsamo et al. 2011). The ERAI reanalysis is produced with a sequential data assimilation scheme, advancing forward in time using 12-hourly analysis cycles. In each cycle, available observations are combined with prior information from a forecast model to estimate the evolving state of the global atmosphere and its underlying surface. This involves computing a variational analysis of the basic upper-air atmospheric fields (temperature, wind, humidity, ozone, surface pressure), followed by separate analyses of near-surface parameters (2m-temperature and 2m-humidity), soil moisture and soil temperature, snow, and ocean waves. The analyses are then used to initialise a short-range model forecast, which provides the prior state estimates needed for the next analysis cycle. The data assimilation thus produces a coherent record of the global atmospheric evolution for the entire period of reanalysis, which is consistent with available observations. The ERAI archive contains 6-hourly gridded estimates of 3-dimensional meteorological variables, and 3-hourly estimates of a large number of surface parameters and other 2-dimensional variables, and is freely available in the full resolution at: http://data-portal.ecmwf.int/data/d/interim_full_daily

The CAMSOPI is a merged dataset produced by the NOAA Climate Prediction Centre (CPC) combining satellite rainfall estimates from the Outgoing Longwave Radiation (OLR) Precipitation Index (OPI) with ground-based rain gauge observations from the Climate Anomaly Monitoring System (CAMS). The OPI estimates are computed from NOAA polar-orbiting IR window channel data using the technique developed by Xie and Arkin (1998). While it is recognized that the OPI has significant limitations for many climate applications, the merged CAMSOPI dataset was developed primarily requiring near real-time applications. For research purposes, CPC encourage users (http://www.cpc.ncep.noaa.gov/products/global_precip/html/wpage.cams_opi.html) to use either the GPCP (Huffman et al. 2009) or CMAP (Xie and Arkin 1997) merged climate rainfall datasets, both of which have better quality control measures and include satellite passive microwave rain estimates. Janowiak and Xie (1999) provide a complete description of the CAMSOPI merged dataset, that is available from January 1979 to present in a 2.5°x2.5° lat/lon regular grid at the CPC ftp site (ftp://ftp.cpc.ncep.noaa.gov/precip/data-reg/cams_opi_v0208).

In-situ observations of precipitation from rain-gauges are spatially and temporally scarce in Africa. We use the Global Precipitation Climatology Project (GPCP) version 2.2 (Huffman et

al. 2011) monthly precipitation which is available since Jan 1979 to Dec 2010 on a 2.5°x2.5° lat/lon regular grid. Throughout the report this datasets is assumed to be the best observational based estimate of precipitation (based on merged rain-gauges and satellite data), and is considered as the benchmark observations.

2.1.2 Seasonal forecasts

Seasonal forecasting provides useful information about the "climate" that can be expected in the coming months. The seasonal forecast is not a weather forecast: weather can be considered as a snapshot of continually changing atmospheric conditions, whereas climate is better considered as the statistical summary of the weather events occurring in a given time period. The principal aim of seasonal forecasting is to predict the range of values which is most likely to occur during the next season. In some parts of the world, and in some circumstances, it may be possible to give a relatively narrow range within which weather values are expected to occur. Such a forecast can easily be understood and acted upon; some of the forecasts associated with strong El Nino events fall into this category. More typically, the probable ranges of the weather differ only slightly from year to year. Forecasts of these modest shifts might be useful for some but not all users.

ECMWF seasonal forecasts, based on an atmosphere-ocean coupled model, were used for the drought forecasting in this report, where we evaluate the recently implemented System 4, which became available in November 2011 (S4; Molteni et al. 2011). The horizontal resolution of the atmospheric model is TL255 (about 0.7° in the grid-point space, same as ERAI) with 91 vertical levels in the atmosphere. The ocean model has 42 vertical levels with a horizontal resolution of approximately 1°. The seasonal forecast generates 51 ensemble members in real-time, with 30 years (1981-2010, 15 ensemble members) of back integrations (hindcasts). The lead time is 7 months, including the month of issue. Molteni et al.(2011) present an overview of the model biases and forecast scores of S4. The DEWFORA report D4.2 provides an overview of the performance of S4 (compared with other 3 seasonal forecasts systems) in predicting precipitation on a pan-African scale.

2.2 RIVER BASIN SELECTION

We selected 5 river sub-basins in Africa to test the drought monitoring and seasonal forecasting methodology. Four of the basins are the part of the DEWFORA case studies: Blue Nile (BN), Limpopo (LP), Upper Niger (NG) and Oum er-rbia (OR), and the fifth basin accounts for the all Congo (CG) basin. The CG was also included due to its central location in Africa with a different precipitation regime. This is an extended evaluation of the capabilities of the dynamical model in representing the precipitation variability in the region, which is related to the pan-African case study. The basins represent upstream basins at a gauging station in the selected main rivers, described in Table 1 and illustrated in Figure 1.

The catchment definitions were taken from the river network and basins created by Yamazaki et al. (2009).

Table 1. Sub-Basins definitions. See also Figure 1.

Basin	Outlet	Area (x 10^5 km^2)
Blue Nile (BN)	15.5°N, 32.68E	3.2
Congo (CG)	-4.1°N, 15.5E	36.4
Limpopo (LP)	-24.24°N, 32.79E	3.4
Upper Niger (NG)	16.24°N, -3.39E	3.6
Oum er-rbia (OR)	33°N, -8.05E	0.35

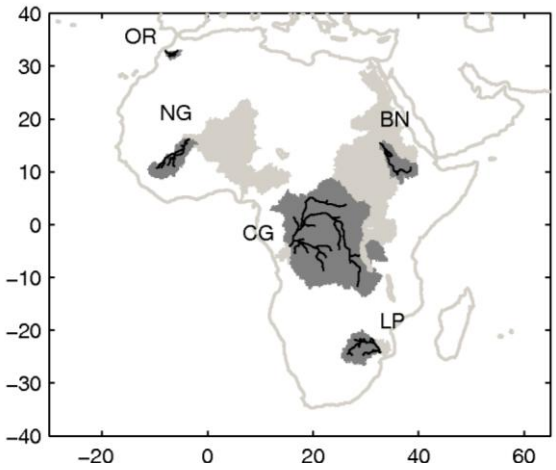

Figure 1. Sub-basins definitions (dark gray) and the full basin (dark and light gray). See also Error! Reference source not found.**.**

A detailed description of the four DEWFORA case studies (NG, LP, BN and OR) including the main meteorological and hydrological features, and the drought related risks and available infrastructures are documented in the DEWFORA D6.1 report

2.3 AFRICA SYNOPTIC

The atmospheric circulation over the Africa continent is to be considered in spatial continuity with conditions over the adjacent Eastern Atlantic. Most of the precipitation over this continent is controlled by the south to north and back displacement of the Inter Tropical Convergency Zone (ITCZ), the intensity of the low level Tropical Easterly Jet (TEJ) and the flow disturbances in the high level African Easterly Jet (AEJ). The interaction of all these large scale features combined with local produced convection generates four climatic zones relevant in terms of large scale precipitation and temperature; the well pronounced West

Africa monsoon system, the less intense East Africa monsoon and the central Africa bi-seasonal variation.

The rainfall field over West Africa is characterised by a zone of maximum precipitation that migrates north and south throughout the course of the year (Figure 2). This zone lies to the south of the ITCZ and its seasonal excursion roughly parallels the seasonal excursion of the ITCZ. The monsoon rain-belt which is responsible for the large scale precipitation is associated with disturbances that are dynamically linked to the African Easterly Jet. Instead westward propagating mesoscale disturbances generate the dominant convective systems. Certain environmental factors, such as vertical wind shear, buoyant energy, low-level jets, and latitude, determine whether these scattered convective events organise into long-lived systems. Although the shear instability associated with the jet is present throughout the rainy season (June to September), mesoscale instabilities feed into the large scale disturbance only during late boreal summer (when enough moisture is available). This fact may help to explain the contrast between the rainfall regimes in June-July (mostly frontal precipitation) and August-September (mostly convective). Areas somewhat south-east of West Africa (Central Africa Republic, Chad, and Sudan) and west (Nigeria and other countries of the Guinea Coast) are meteorological controlled by the same processes and features that influence Sahelian West Africa and peak rainfall occurs in the boreal summer, when the ITCZ moves to its far northern limits. Two basins have been selected in this region, the Niger (NG) and the Blue Nile (BN), experiencing most the precipitation in the June to September period.

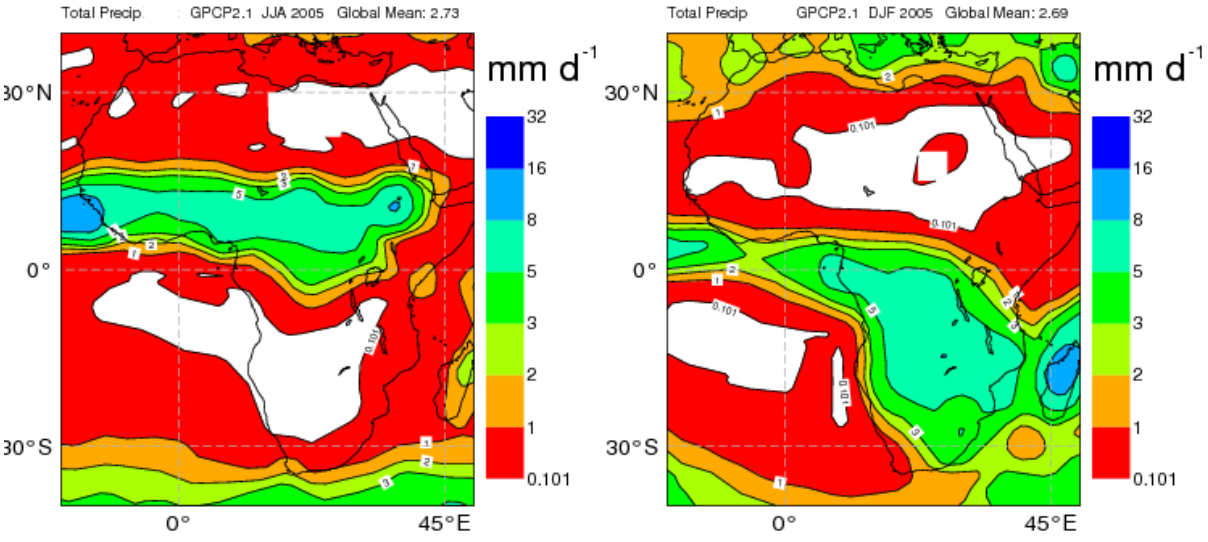

Figure 2. Precipitation for the JJA (left) and DJF (right) from the GPCP v2.1 showing the north-south migration of the ITCZ.

Central Africa extending westward to Cameroon and eastward to the Rift Valley highlands experiences a strongly bimodal annual cycle, coincident with both the northward and southward passage of the ITCZ. Peak rainfall tends to be in the two transition seasons.

The Limpopo river basin (LP) is located in East Africa where a small monsoon cycle is present with peak precipitation occurring during boreal winter. The variance spectra for rainfall throughout this region show very strong peaks on the order of 5-6 years and generally smaller peaks at roughly 3.5 and 2.3 yr, the same peaks found in the Southern Oscillation. The variability is generally out of phase with that in the Sahel (i.e., dry (wet) Sahel corresponds to wet (dry) Central Africa). Although wave activity has not been identified, rainfall tends to be organized into mesoscale convective systems analogous to those in Sahelian West Africa. Very little is still known about the modulation introduced by the Rift Valley highlands on the large scale flow.

2.4 STANDARDIZED PRECIPITATION INDEX (SPI)

In this study we use the Standard Precipitation Index (SPI). The SPI is a commonly used drought index (e.g. Keyantash and Dracup 2002). It is recommended by the World Meteorological Organization as a standard to characterize meteorological droughts (WMO 2009) and by the DEWFORA report D4.2. The SPI is based on the probability of an observed precipitation deficit occurring over a given prior accumulated time period. This time period is defined accordingly to the particular application, with typical values of 3, 6 and 12 months. The flexibility of the accumulation in different time periods allows a range of meteorological, agricultural and hydrological applications. For short accumulations periods, e.g. 3-month, the SPI will reflect short- and medium-term moisture conditions associated with seasonal estimations of precipitation. However, a relatively normal 3-month period (or even wet) can occur during a long drought spell. The 6-month SPI is associated with medium-term precipitation anomalies and is usually associated with anomalous stream flows and reservoir levels. On longer times-scales, the 12-month SPI compares the 12 month consecutive precipitation of a certain year, with all the previous years available, reflecting long-term precipitation patterns, that are associated with changes to large reservoirs and groundwater. Despite the general association of SPI time-scale with soil moisture, stream-flow and ground water changes, such relations are regionally dependent on the precipitation regime and geological characteristics, among others. In each particular region/application, a detailed study (as possible, when data is available) should be carried out to relate the different SPI time scales with the target variable, such as soil moisture available to crops or natural reservoirs.

Lloyd-Hughes and Saunders (2002) identified three potential disadvantages with SPI: (i) the assumption of a theoretical probability distribution function associated with the quantity and reliability of the data used (ii) the SPI is not capable of identifying regions more prone to drought than others and; (iii) for short time scales (1 to 3 months) misleadingly large positive or negative SPI values may appear in regions of low seasonal precipitation. Mckee et

al.(1993) recommended at least 30 years of high-quality data to minimize the uncertainties in fitting the theoretical distribution to the data.

In the calculation of the SPI for a specific *k* time-scale the total precipitation for a certain month *m (m=1,…,N,* where *N* is the number of months in the time series) is the sum of the precipitation for the period: [*m-k+1 to m*] (see Figure 3). For each calendar month (i.e. all Januaries, Februaries,...) the accumulated precipitation distribution (N/12 samples) is fitted to a probability distribution. The resultant cumulative probability distribution (CDF) is then transformed into the standard normal distribution (mean zero with one standard deviation), resulting in the SPI (see Figure 4).

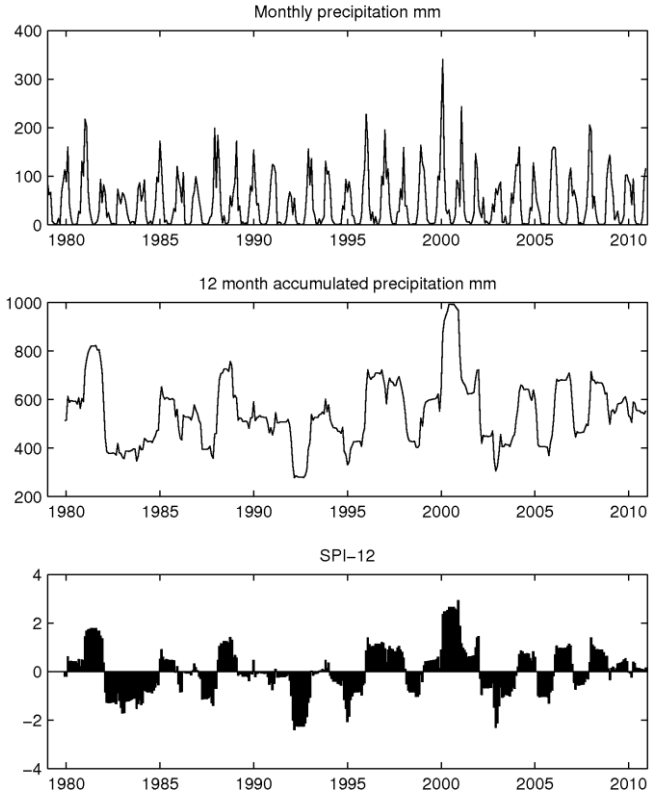

Figure 3. Example of the transformation of a monthly precipitation time-series (top) to 12-month accumulated precipitation (middle) and it's standardization to the SPI-12 (bottom).

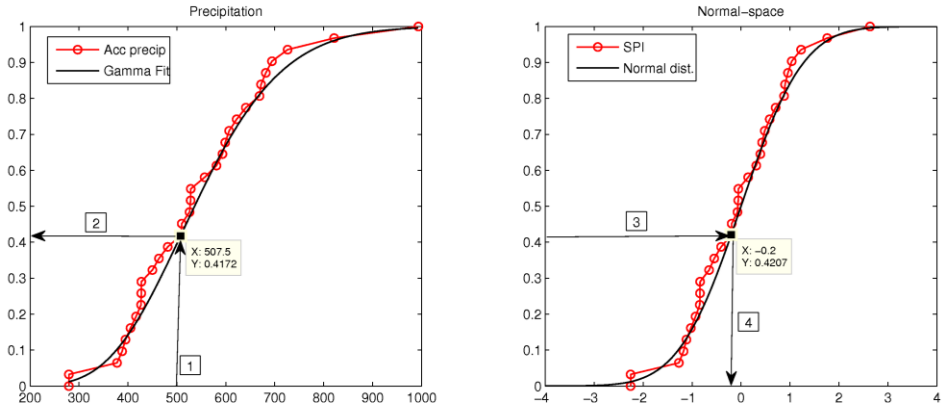

Figure 4. Left: empirical cumulative distribution function -CDF (red) of 12-month accumulated precipitation (see Figure 3) and the best fit using a gamma distribution (black). Right: Transformation to a

normal distribution of mean zero and standard deviation 1 (black) of the gamma fitted 12-month accumulated precipitation CDF (red).

It is common to select a parametric probability distribution to fit the precipitation. Different statistical distributions can be used, such as the gamma distribution (Lloyd-Hughes and Saunders 2002) or Pearson III (Vicente-Serrano 2006), and there are statistical tests (e.g. Kolmogorov-Smirnov) to assess the suitability of the selected distribution to the precipitation data. Depending on the selected probability distribution, the parameters estimation can be done using known analytical approximations or by optimization algorithms. In the present work we have selected the gamma function, and the fitting uses the approximation proposed by Greenwood and Durand (1960). Different probability distribution functions or different parameters estimation methods can be used, but such an analysis is beyond the scope of this work.

The extension of the SPI from the monitoring period, i.e. past, to the seasonal forecast range, is performed by merging the seasonal forecasts of precipitation with the monitoring product. The method can be resumed in three general steps:

1. Downscale or upscale the forecasts of precipitation to the target resolution

In the present work both the monitoring and seasonal forecasts of precipitation were spatially aggregated over the basins (see Table 1), instead of performing the calculations and evaluation on a grid-point base. The spatial aggregation reduces the amount of data to process, but also filters some of the intrinsic noise of grid-point precipitation from dynamical models. The spatial aggregation is performed in three steps: (i) definition of the basin mask on a 0.25x0.25 grid (about 3 times higher than the original ERA-Interim and S4 and 10 times CAMSOPI); (ii) bilinear interpolation of the precipitation products to the 0.25x0.25 grid and (iii) spatial averaging of the interpolated data over the basin mask. This procedure can be applied to any basin/region depending only on a high resolution mask/outline. If the method is to be applied on a grid-point scale, or even local station, other statistical methods of downscaling (and bias correction – see next point) can be applied.

2. Bias correct the seasonal forecast

Dynamical atmosphere-ocean seasonal forecasts of precipitation (and other variables) tend to have significant biases and sometimes drifts, i.e. the bias changes with lead time (for example see Figure 5 showing the change of the mean annual cycle of monthly precipitation in S4 with lead time in the selected basins). When merging the monitoring with the seasonal forecasts, the mean climate of the forecasts should be similar to the monitoring. We apply a simple multiplicative factor correction to the monthly precipitation, for each lead time and initial forecast month. The procedure corrects the mean S4 climate for all initial forecast dates and lead time, but does not address inter-annual variability and ensemble spread.

More sophisticated bias correction methods, such as quantile match, patterns regression, could be applied, but is not clear if such methods could be beneficial for the present application. Furthermore, the applied method does not interfere with the spatial patterns generated by the dynamical model. These can be biased, but are physically consistent.

3. Merging the monitoring and forecasts of precipitation to create the accumulated precipitation and calculate the SPI

The interpolated and bias-corrected S4 precipitation (points 1 and 2) was then merged with the monitoring to create a seamless extension of the monitoring with the forecast. This was performed for the entire hindcast period and the resultant cumulative probability distributions, for each calendar month (450 samples 30 (years) x 15 (ensemble members)) and lead time (1 to 7 months), were transformed into normal space using the same method as described before for the SPI monitoring.

Yoon et al. (2012) recently proposed a similar methodology to forecasts 3- and 6-month SPI for the prediction of meteorological drought over the contiguous United States based on precipitation seasonal forecasts from the NCEP climate forecast system (CFS). In their application, the precipitation forecasts from the coarse-resolution CFS global model were bias corrected and downscaled to a regional gird of 50 km. Here we propose an upscaling of the seasonal forecast to basin scale which filters the intrinsic noise of grid-point precipitation forecasts. Yoon et al. (2012) tested five downscaling methods: i) bilinear interpolation, ii) bias correction and spatial downscaling (BCSD) based in the probability distribution function, iii) a conditional probability estimation approach using the mean P ensemble forecasts (Wood and Schaake 2008), iv) a Bayesian approach that bias correct and downscales precipitation using all ensemble forecasts members (Luo et al. 2007) and v) a multi-method ensemble. The authors found that the skill was regionally and seasonally dependent, with an overall skill out to 3-4 months of the 6-month SPI, where in the first 3-month lead times, forecast skill came from the precipitation analysis prior to the forecast time. Furthermore, the different downscaling methods produced different precipitation anomalies, but the differences were not large enough to make a difference in the SPI prediction, concluding that the SPI prediction skill came mainly from the precipitation analysis appended to the forecasts.

3. RESULTS AND DISCUSSION

3.1 MODELS CLIMATE

The GPCP mean annual cycle of precipitation in the different basins was compared with ERAI, CAMSOPI and S4 in Figure 5. In the BN and NG the rainy season (June-Sep) is captured by all datasets, whereas in BN ERAI shows a significant overestimation and CAMSOPI is in good agreement with GPCP. S4 forecasts overestimate precipitation in both BN and NG basins in the first forecast month with a reduction of the peak rainfall with lead time, showing the impact of model drift. In the large CG basin, ERAI, CAMSOPI and S4 show an early peak rainfall in March (GPCP in April) and a latter peak in November (GPCP in October). ERAI generally overestimates precipitation in CG, while S4 overestimates its amplitude. In the LP and OR basins all datasets show a reasonable agreement, with an underestimation of the rainy season in OR, and S4 has a reduced drift on both basins.

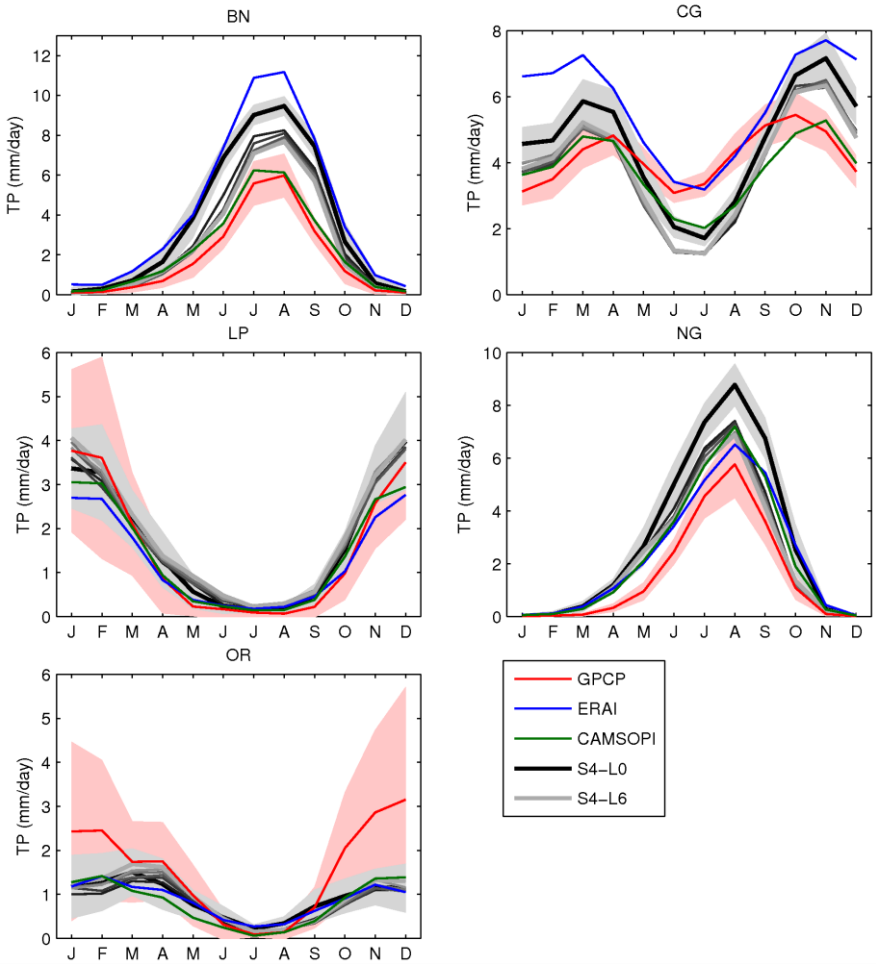

Figure 5. Mean annual cycle of precipitation over the selected basins. The shaded area shows the range (+/- 1 standard deviation) of observed (GPCP-red) and modelled (S4-gray) precipitation over the regions for the hindcast period 1981-2010, comparing with ERAI (blue) and CAMSOPI (green). The time series for the seasonal forecast uses the first month of forecast (lead time 0) and the 15 forecast ensemble members (gray area and thick black), the last month of forecast (lead time 6) in thick gray, and the remaining lead times in thin gray.

The mean annual cycle reflects the general behavior and systematic biases of the datasets, but for drought applications the timing of the rainy seasons and its interannual variability (Figure 6) are the key factors. Systematic biases are not reflected in the SPI (since it is a normalized measure), but errors in the timing, amplitude and variability will degrade the ability of the dataset to monitor (ERAI, CAMSOPI) and forecast (S4) meteorological droughts. From the mean annual cycle analysis, CG basins appear as the most problematic with timing errors in the rainy season, and amplitude problems in S4.

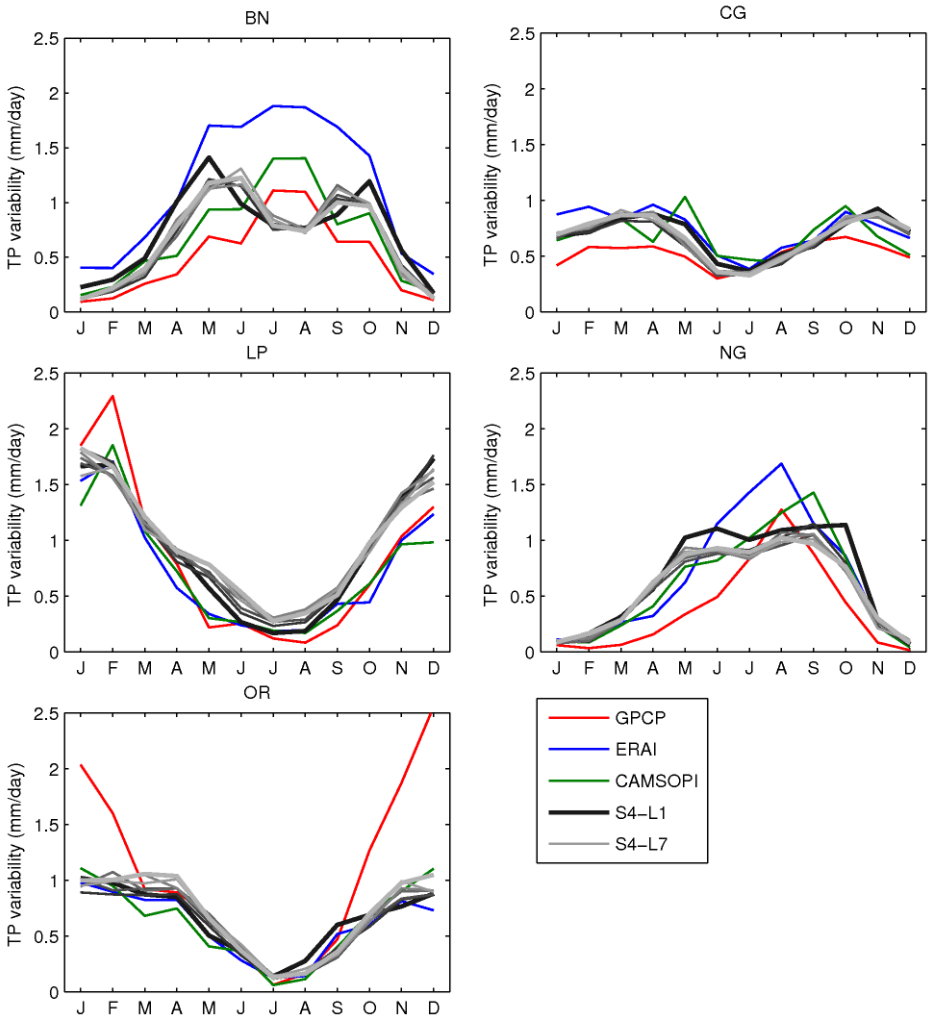

Figure 6.Inter-annual standard deviation of monthly precipitation over the selected basins. Observed (GPCP-red) compared with ERAI (blue), CAMSOPI (green) and S4 for the first month lead time (thick black), 7 months lead time (thick gray) and the remaining lead times (thin gray lines). The S4 standard deviation is takes for each month and lead time considering all the ensemble members (15) and not the ensemble mean.

The inter-annual variability is evaluated as the monthly standard deviation (i.e. variability of a certain month in different years) (Figure 6). The annual cycle of monthly inter-annual variability has a similar behavior to the mean annual cycle of precipitation in all basins. In the BN and NG, the ERAI overestimation of precipitation is also reflected in higher inter-annual variability, while in the CG and LP there is a good agreement between ERAI, CAMSOPI and

GPCP. The underestimation of precipitation during winter in OR by all datasets is also associated with lower inter-annual variability. The changes in variability with lead time in S4 are smaller than what was found for the mean annual cycle of precipitation. This supports the simple bias correction of the mean that was applied to S4 with lead time. However, in both BN and NG S4 do not represent the sharp peak variability from June to September, and in the BN July-August have less variability than May or September. The underlying reasons for this behavior are unknown, but can be related with a lack of regional-scale interactions (e.g. with orography, soil moisture) that amplify/damp large scale anomalies.

3.2 DROUGHT MONITORING

The temporal evolution of the SPI-12 and SPI-3, based in GPCP, are shown in Figure 7. The SPI-3 has a high temporal variability that is associated with short-to-medium range meteorological anomalies that can be reflected on soil moisture and crops evolution. The long-term anomalies in SPI-12 point to several major drought events: BN:1983-85; 1991-92; 2010; CG: 1984-85, 1994, 2004, 2009; LP: 1982-84, 1992, 2002-03; NG: 1983-86, 1991; and OR: 1981, 1995, 1999, 2005. These dates have a reasonable agreement with the data compiled in the D2.2 DEWFORA report. Different SPI time scales can be analysis in more detail, as well has their regional patterns to further access the agreement with reported droughts. Such analysis is out of the scope of the present report.

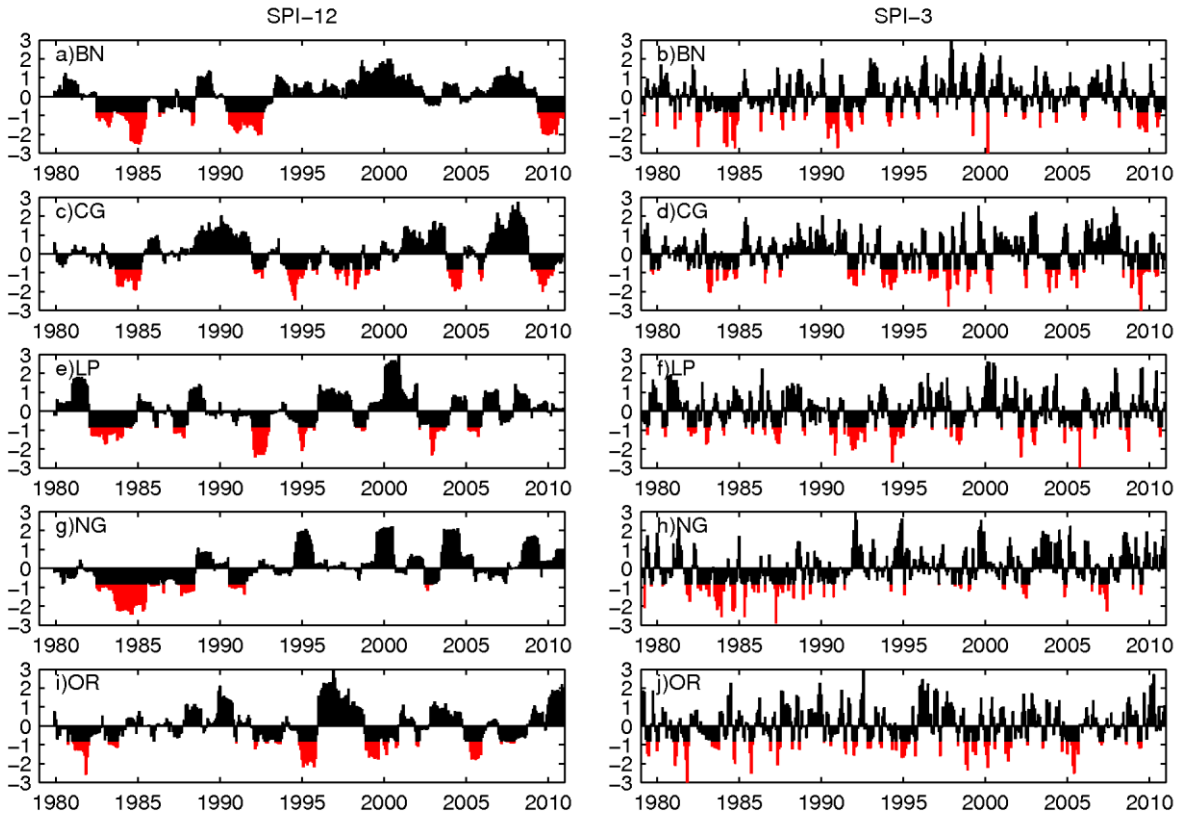

Figure 7. Evolution of the 12-month (left panels) and 3-month (right panels) SPI in the different basins. Highlighted areas correspond values bellow -0.8 associated with moderate to severe droughts (Svoboda et al. 2002).

The comparison of the SPI-12 calculated from, ERAI, CAMSOPI and GPCP for the different basins is presented in Figure 8, while the temporal correlation of the different SPI-time scales between the different datasets is shown in Figure 9. In the LP in OR basins, there is a good agreement in the temporal evolution of the SPI at different time scales between GPCP and ERAI and CAMSOPI. In the BN and NG the temporal correlation of both ERAI and CAMSOPI compared with GPCP decays with increasing SPI time-scale. These results show inconsistencies of the inter-annual variability between GPCP and the two datasets that penalize the SPI on long accumulation time-scales. The inconsistency is obvious as the accumulation time increases (>6 months), but for the shorter accumulation times, the temporal correlation is seemingly higher. This can however be an artefact of the SPI, which normalises the values and gives equal weight to anomalies in the dry season, which are of little importance.

The inconsistency is also the case for ERAI in CG, but not for CAMSOPI. In the NG, both ERAI and CAMSOPI show an opposite trend to GPCP, with a wet period until 2000 and severe and long term drought in the last decade. For this reason, the correlations between GPCP and ERAI and GPCP and CAMSOPI in the NG are very low, but high when comparing ERAI and CAMSOPI (Figure 9). This feature of ERAI and CAMSOPI will be further discussed latter.

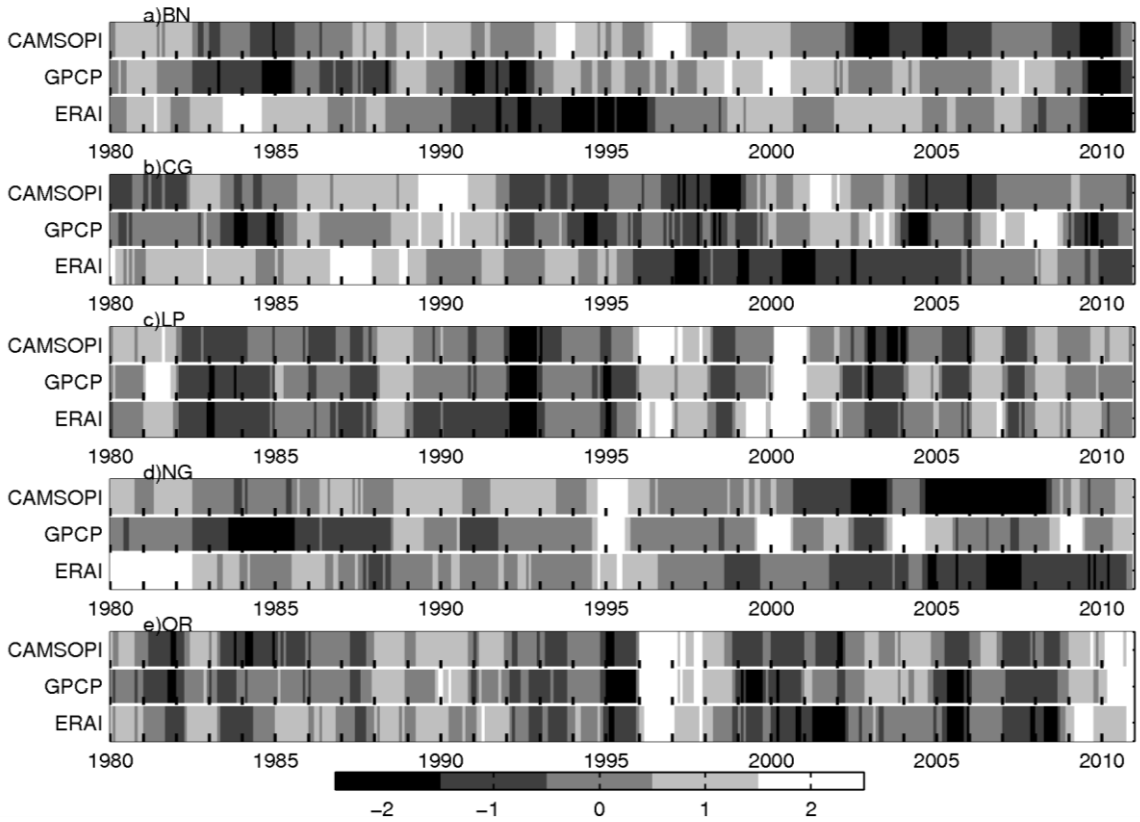

Figure 8. Evolution of the 12-month SPI in the different basins given by CAMSOPI, GPCP and ERAI. The horizontal ticks represent January of each year.

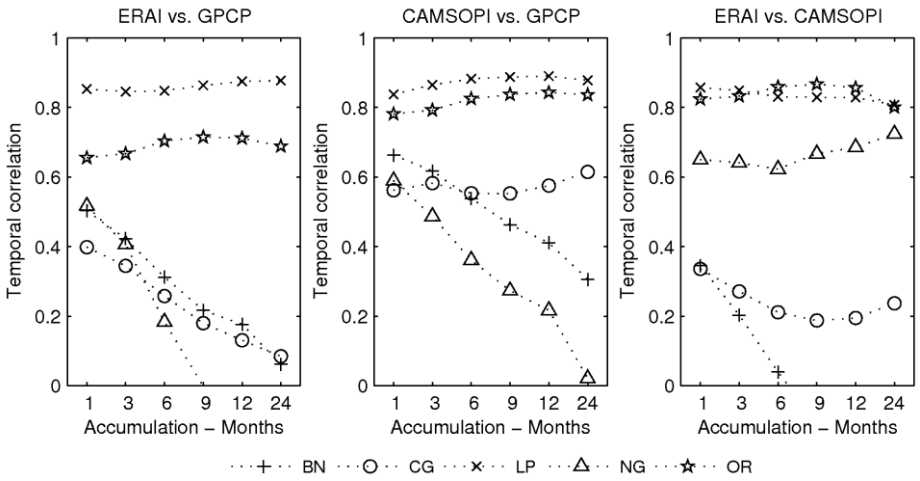

Figure 9. Temporal correlation of (left) ERAI and GPCP, (centre) CAMSOPI and GPCP and (right) ERAI and CAMSOPI n-months SPI (horizontal axis) for the five basins (symbols).

The spatial distribution of temporal correlations of the SPI-3 and SPI-12 calculated from the different products are presented in Figure 10. All the datasets show a good agreement in the South and North West, while in Central Africa (between the +/- 20° parallels) ERAI and CAMSOPI have low correlations, especially for long accumulation periods. However, CAMSOPI tends to have a better agreement with GPCP than ERAI.

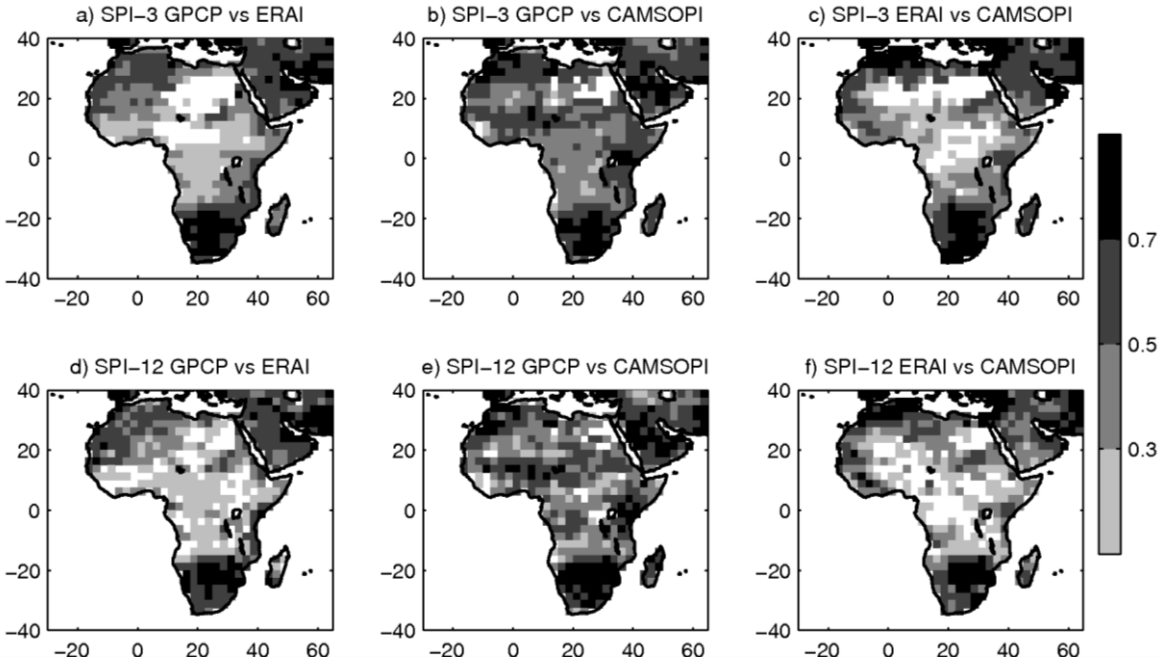

Figure 10. Temporal correlation of (a-c) 3-month and 12-month (d-f) SPI of (a,d) GPCP and ERAI, (b,e) GPCP and (c,f) CAMSOPI and ERAI and CAMSOPI.

With the accumulation of precipitation on different time scales, the SPI temporal evolution can be approximated to an autoregressive model of 1th order: $X_m=\alpha X_{m-1}+\varepsilon_m$ where X is the SPI, the subscript the month, ε a white noise of zero mean, and α the model parameter. The autocorrelation decays with a decay time $\tau=-1/\ln(\alpha)$, in the form: $\exp(-m/\tau)$. The autocorrelation of the SPI-12 is represented in Figure 11 for each basin, and Table 2 displays

the associated autocorrelation decay time scales τ (months) and variance of white noise $\sigma^2\varepsilon$. In all basins, except OR, GPCP has lower decay time scales and higher variance of white noise while ERAI has the higher time scales and lower white noise variance. In OR all three datasets have a similar behaviour. The decay timescale can be associated to a measure of the persistence of an anomaly that tends to be higher in both ERAI and CAMSOPI, when compared with GPCP.

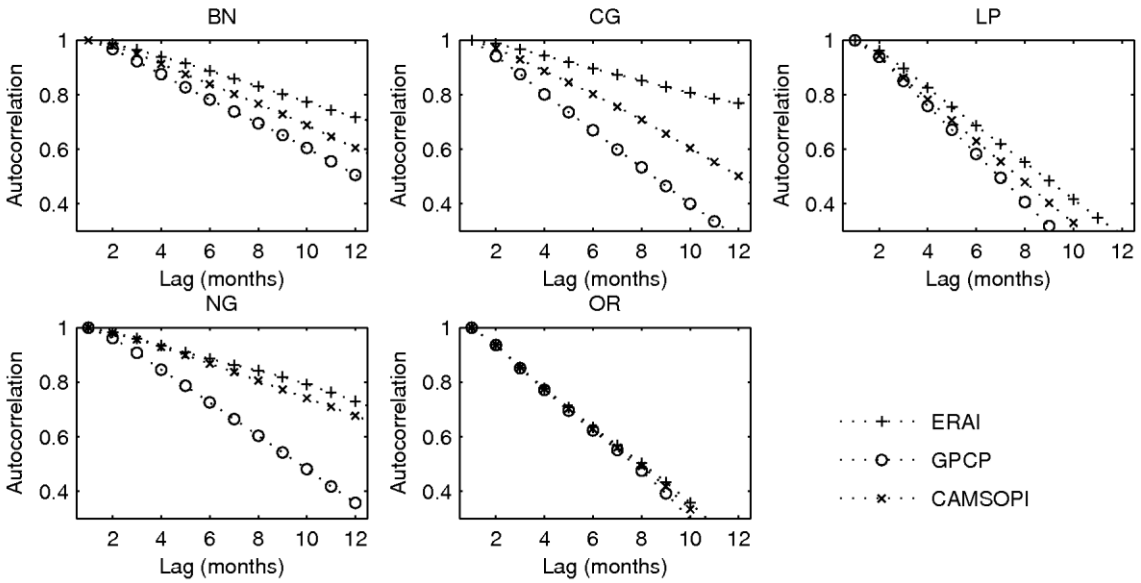

Figure 11. Temporal autocorrelation of the 12- months SPI calculated using ERAI (cross), GPCP (circle), and CAMSOPI (star) for the different basins.

Table 2.SPI-12 autocorrelation decay time scale τ (months) and variance of white noise $\sigma^2\varepsilon$

	ERAI		GPCP		CAMSOPI	
	τ	$\sigma^2\varepsilon$	τ	$\sigma^2\varepsilon$	τ	$\sigma^2\varepsilon$
BN	33.8	0.06	13.2	0.14	21.7	0.09
CG	33.8	0.04	11.7	0.16	21.1	0.1
LP	11.7	0.16	8.0	0.23	10.4	0.18
NG	18.8	0.09	9.5	0.19	22.0	0.09
OR	9.7	0.19	7.2	0.24	9.0	0.20

The selection of the SPI time-scale will depend on the particular application. The time-scale selection can be performed by comparing the temporal anomalies of SPI in different time scales with the target variable, such as soil moisture, crop production, river discharge, etc. This comparison can be also used as a qualitatively evaluation the SPI capabilities in capturing agricultural and/or hydrological droughts. In Figure 12 we compare the different SPI time-scales for each calendar month against the river discharge anomalies from

observations in the NG basin. Our results show a good agreement between the GPCP derived SPI at time-scales higher than 5/6 months, for all calendar months except July, when compared with river discharge anomalies. For example, the SPI-12 in June (accumulated precipitation from May of the previous year to June of the current year) has a high correlation with the June stream-flow in the basin outlet (centre panel of Figure 12). However, when comparing the SPI derived from ERAI and CAMSOPI with stream-flow, the correlations are much lower or no-existent. This can be interpreted as an indirect verification of the ERAI and CAMSOPI SPI, reflecting the poor intra-seasonal to inter-annual variability of precipitation of those datasets in the NG region. Figure 19 and Figure 20 compare the SPI with river discharge in the OR and CG basins, respectively. The SPI comparison with river discharge in the CG basins is in agreement with the findings of Vicente-Serrano et al. (2012). Similar analysis could be also performed with the extension of flooded areas (for example using the dataset developed by Prigent et al. (2007)).

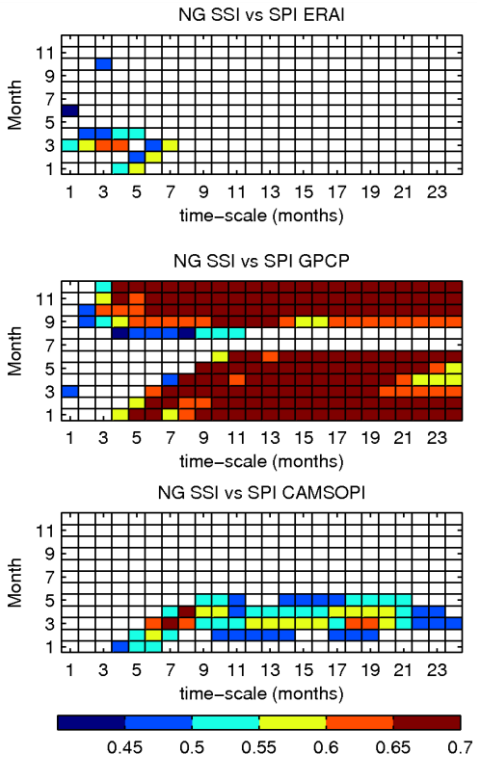

Figure 12. Correlations between Stream-flow (z-score) and the 1- to 24 month SPI from ERAI (top), GPCP (middle) and CAMSOPI (bottom) in the NG basin. Observations from GRDC station DIRE.

3.3 SEASONAL FORECASTS

We start by analyzing the skill of S4 precipitation forecasts in terms of the anomaly correlation coefficient (ACC) for the ensemble mean for each basin. The 3-month ACC for each forecast month as a function of lead time is represented in Figure 13, and the monthly ACC in Figure 14. In the BN, LP and NG basins, the seasonal forecasts have skill up to 3

months lead time for the rainy seasons, while in the CG and OR basins S4 does not have skill.

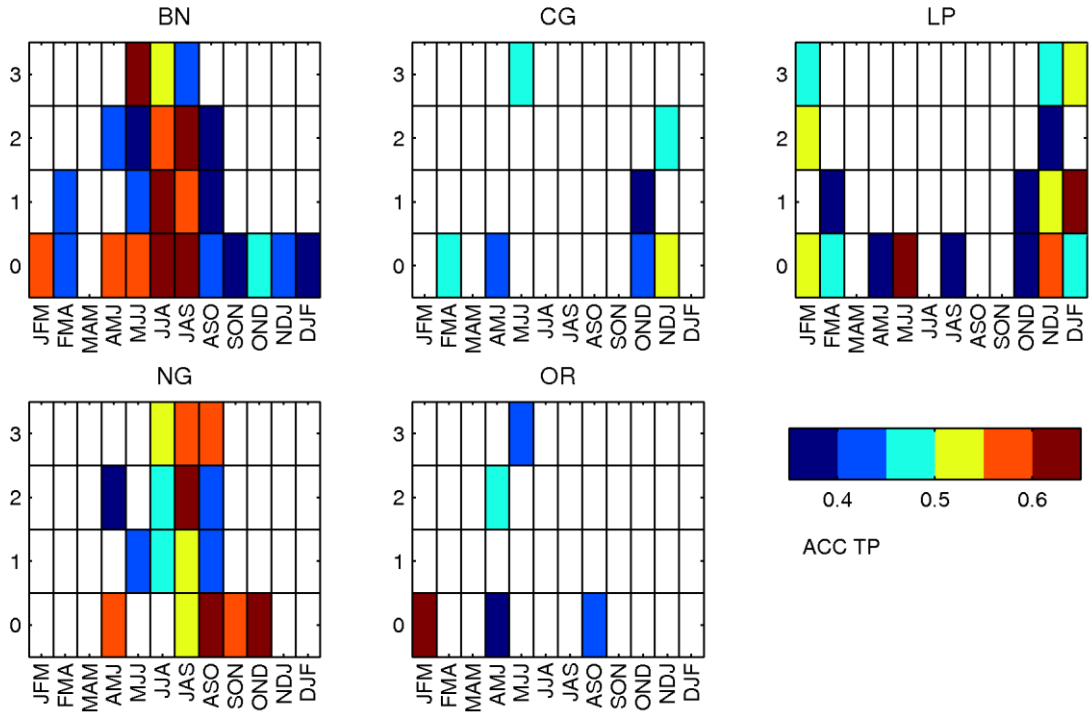

Figure 13. Anomaly correlation coefficient S4 3-months total precipitation as a function of verification season (horizontal axis) and lead time (vertical axis) for the different basins. Only ACC significant at p<0.05 are displayed. For example, the values valid at JJA with lead time 0 (3) corresponds to the forecasts starting in June (March). The forecasts were verified against GPCP for the period 1981 to 2010.

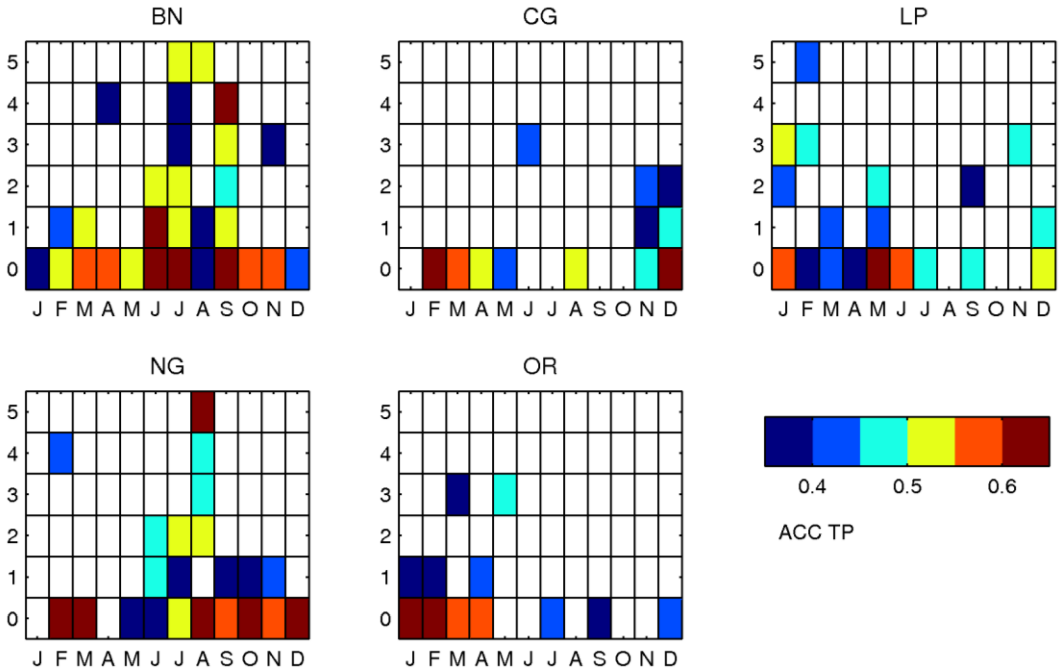

Figure 14. As Figure 13 but for monthly precipitation.

For the SPI seasonal forecasts, we start by assessing the potential skill, i.e. considering that we have access to a perfect monitoring, in this case GPCP (also used as verification). The

ACC and the continuous rank probability skill score (CRPSS) of the SPI-3,6, and 12 are represented in Figure 15 as a function of lead time for the entire time series (30 years handcarts). The continuous rank probability score (CRPS, see Hersbach (2000)) is a development of the Ranked Probability Score (RPS). It can be interpreted as the integral of the Brier Score over all possible threshold values of the parameter under consideration. In deterministic forecasts, the CRPS is reduced to the mean absolute error. Since the CRPS is not a normalized measure, we evaluate the CRPS skill score (CRPSS). In the skill score calculation the reference forecast (or climatology, CLM) is taken from the verification dataset as sample of different years, to produce a climatological forecast with the same ensemble size as S4, and is merged with the monitoring product, in the same ways and the S4 SPI forecasts. The sampling is not random. It searches in the 30 years of record for 15 (size of the ensemble during the hindcast period) years with similar precipitation amounts during the monitoring.

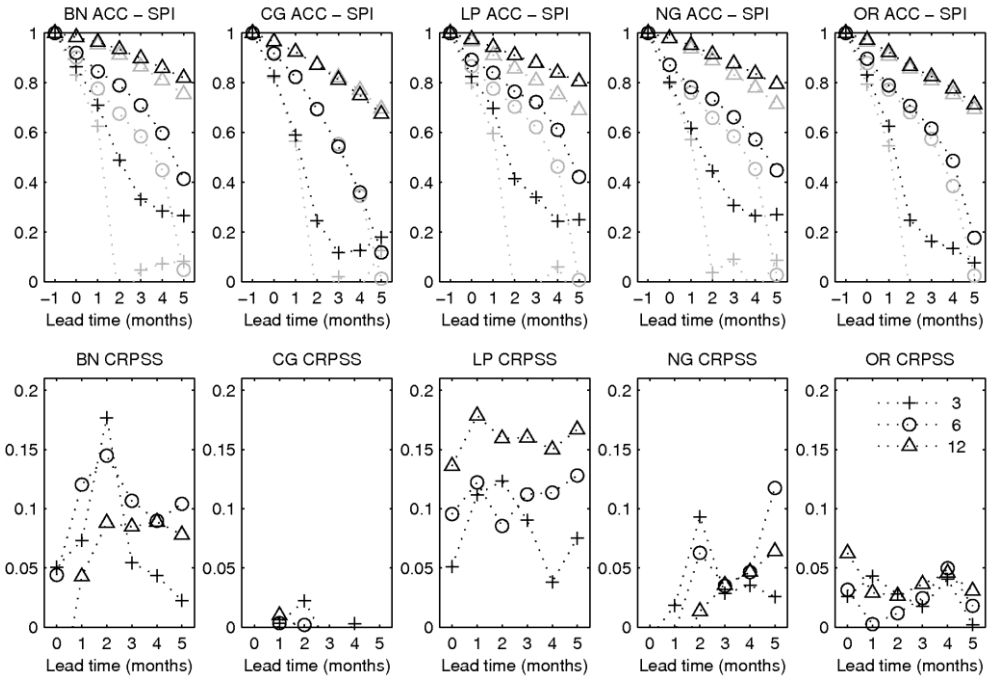

Figure 15. Anomaly correlation coefficient (top panels) and CRPSS (bottom panels) of S4 (black) and climate (gray) SPI forecasts as a function of lead time for different accumulation times (symbols). GPCP is used for the monitoring and GPCP as verification (ACC == 1 for -1 lead time).

The ACC of the SPI decays in time at a faster rate for lower accumulation periods, where the monitoring importance is reduced or inexistent (Figure 15 upper panel). S4 outperforms the climatological forecasts (CLM) in the basins where the original seasonal forecasts of precipitation have skill (Figure 15 lower panel).: BN, LP and NG. In CG and OR, S4 has a similar skill to CLM. However, for long SPI accumulations periods S4 (and CLM) forecasts can potentially provide useful skill due to the dominance of the monitoring (e.g the SPI-12 at 5 months lead time merges 6 months of monitoring and the first 6 months of the forecast). In this situation, the quality of the monitoring will dominate over the skill of the precipitation

forecasts. These skill evaluations can be decomposed in terms of initial forecast month, as it is shown for the LP basin in Figure 16, the OR in Figure 21, the NG in Figure 22, the CG in Figure 23 and the BN in Figure 24.

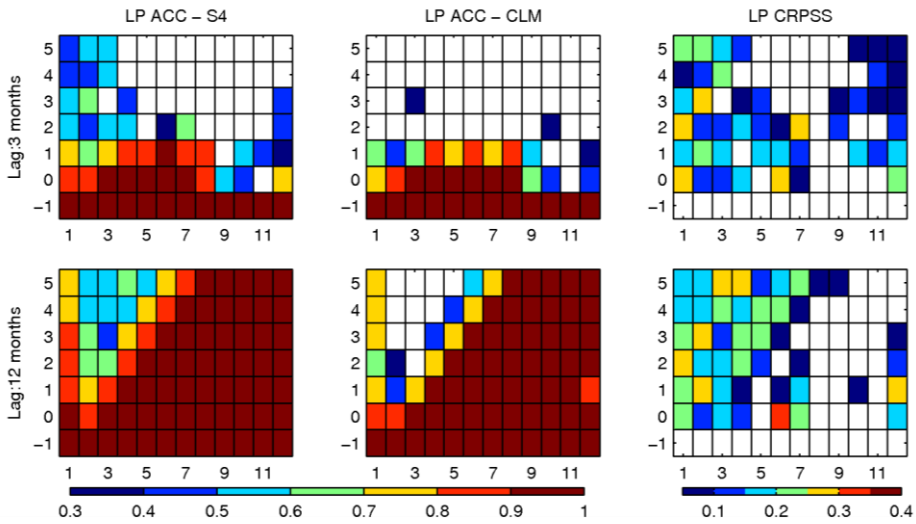

Figure 16. Anomaly correlation coefficient of S4 (left), and climate forecast (centre) and CRPSS (right) of the 3-month (top) and 12-month (bottom) SPI as function verification calendar month (horizontal axis) and lead time (vertical axis) for the LP basin and for different accumulation periods (lines). Lead time -1 represent the skill of SPI on the monitoring period using GPCP, and verified against GPCP. In this situation, the ACC for lead time -1 (monitoring) is equal do 1.

The previous skill analysis, based on ACC and CRPSS, considered the full range of SPI forecasts. For drought detection/early warning, the Relative Operating Characteristics (ROC) score is a useful tool. ROC is a means of testing the skill of categorical forecasts. The derivation of ROC is based on contingency tables giving the hit rate (HR) and false alarm rate (FAR) for deterministic or probabilistic forecasts. The events are defined as binary, which means that only two outcomes are possible, an occurrence or non-occurrence. The Probabilistic ROC score is simply calculated using the HR and FAR. The HR and FAR are calculated for each probability interval. In this case an event is said to be forecast at a point if the forecast probability for an event occurred within the probability range. (e.g., a forecast for an SPI<-0.8 that had a 43% probability would fall in the 40-50% probability range.) Observed occurrences (i.e., Hits) are then the number of times that a forecast probability fell in that bin and subsequently that event occurred (in the example case above an SPI<-0.8 occurred), while the observed non-Occurrences (i.e., Misses) are the number of times a forecast was made for that probability bin but the forecast was "incorrect. The area under the ROC curve is a summary statistic representing the skill of the forecast system. The area is standardized against the total area of the figure such that a perfect forecast system has an area of 1 and a curve lying along the diagonal (no information) has an area of 0.5.

Figure 17 represents the FAR versus HT of the 5 month lead time SPI-6 (first 6 months of forecasts – no monitoring used) and SPI-12 (merged 6 months of monitoring with the first 6

months of forecasts) for the different basins of S4 and CLM. The event is defined when the SPI is below -0.8, representing moderate to severe droughts. For the SPI-6 the ROC of CLM is close to 0.5 (no information), while with S4 the ROC is higher close to 0.7 in the BN, LP and NG, 0.6 in CG and 0.54 in OR. For the SPI-12 the ROC of CLM is always above 0.5, since the climatological forecast inherits 6 months of monitoring. In this case, it is difficult to beat the climate forecast, but S4 outperforms CLM in the BN, LP and NG basins (as documented before).

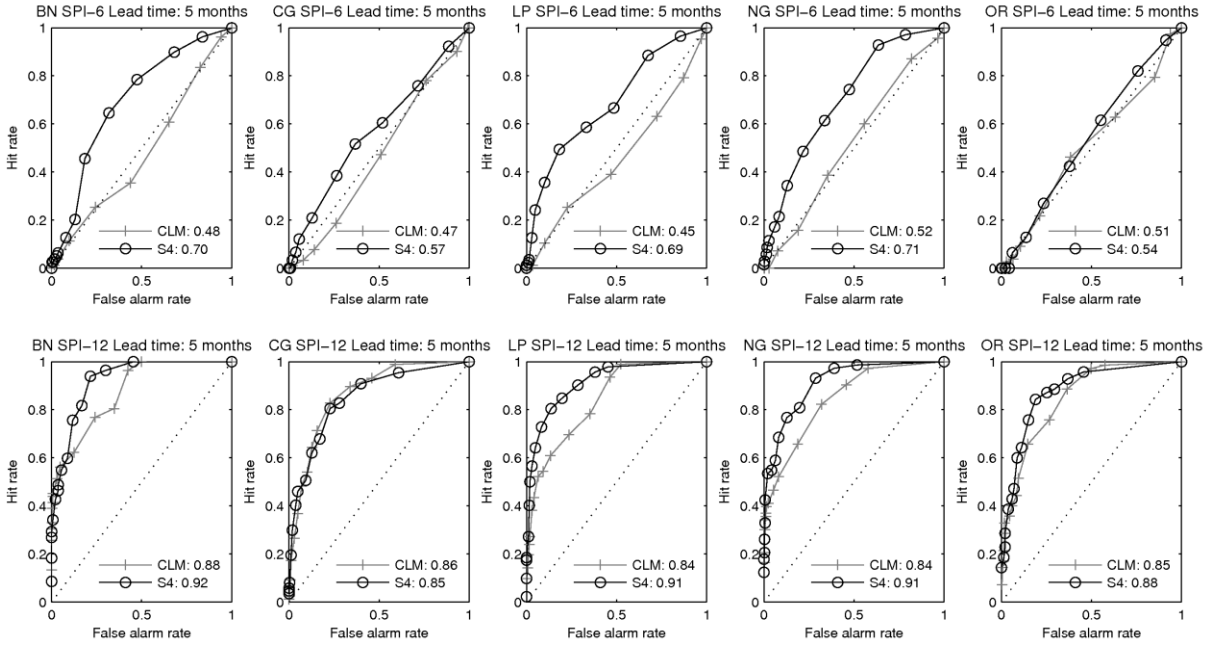

Figure 17. Relative operating characteristic (ROC) diagram representing false alarm rate versus hit rate for the 6 month (top) and 12 month (bottom) SPI <= -0.8 given by S4 (black) and CLM (gray). ROC values are given in the legend of each panel. Calculations based on 20 thresholds (fraction of ensemble members below -0.8), from 1 (symbols closer to 0,0) to 0 (symbols closer to 1,1).

In the previous discussion, only the potential skill was accessed, by using GPCP as monitoring and verification. Since GPCP is not available on near-real time, for an operational implementation other monitoring dataset should be used. Here we use CAMSOPI, since it was shown (see previous section) that it outperformed ERAI. The results presented in Figure 15 are replicated in Figure 25 but using CAMSOPI instead of GPCP for monitoring. There is a significant drop in the ACC, especially in the BN, CG and NG basins. In these basins, it was found that CAMSOPI has problems in representing the intra-seasonal to inter-annual variability of precipitation. These problems, present during the monitoring periods, are extended to the forecast period. Further analysis of the ACC for different initial forecast dates (Figure 26, Figure 27, Figure 28, Figure 29, Figure 30), and ROC scores (Figure 31), highlight the important role of quality monitoring products, that control the skill of the SPI forecasts for accumulation time scales.

We finish this section illustrating the seasonal forecasts of the 1991/92 drought in the LP basin. In Figure 18 each panel corresponds to a different initial forecast date (from August 1991 to July 1992), comparing the SPI-12 from GPCP (verification), CAMSOPI (monitoring) and the S4 and CLM plume forecasts. The drought started to be moderate in January 1992, and severe from February 1992 to November 1992. The forecasts early in September 1991 pointed to a dry anomaly, that was persistently forecasted in October and December 1991, while in November 1991 S4 was similar to CLM forecasting a moderate drought to March 1992. After the drought onset, the March and April 1992 forecasts pointed to an early recover, that was not observed, while the forecasts of May, June and July correctly predicted the start of the recover from September/October 1992 onwards. For the drought recovery period, the S4 forecasts were similar to CLM.

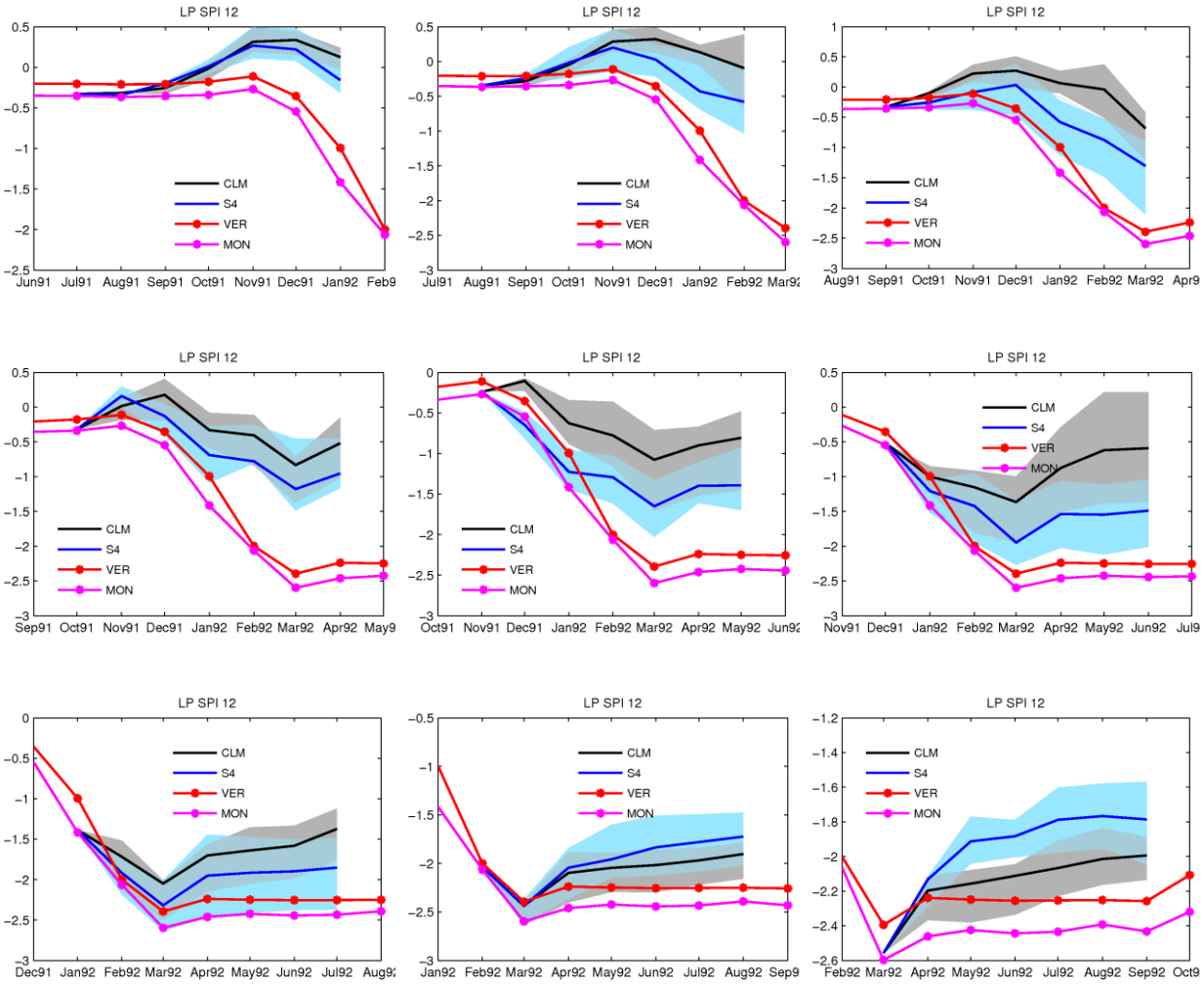

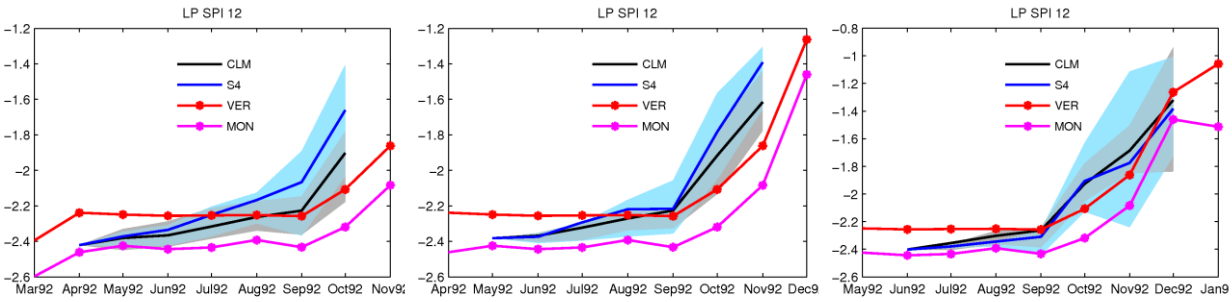

Figure 18. Seasonal forecasts of 12-month SPI for the Limpopo given by system 4 (S4-blue), Climate (CLM, gray), and observed from GPCP (VER, red) and CAMSOPI (MON, magenta). The shaded areas represent the ensemble distribution between the percentiles 30 to 70.

4. SUMMARY AND CONCLUSIONS

In this paper we investigate the use of different observational (GPCP v2.2 and CAMSOPI) and reanalysis datasets (ERA-Interim) as monitoring tools for droughts in a number of African basins. We also test the skill of the new seasonal forecast (SYSTEM 4) in forecasting drought on a seasonal scale, both in combination with reanalysis/observations and as a stand-alone tool.

4.1 MONITORING DROUGHTS

There is a clear difference in skill of monitoring precipitation anomalies, and thereby alos droughts, depending on region. In general, monitoring is difficult in the tropical convergence zone, and the difference datasets show the highest divergence in this regions. It is therefore important to carefully assess the performance of the monitoring dataset for the specific region of interest. The temporal correlation shows that there seems to be a longer “memory” in the ERA-Interim than in the GPCP. GPCP also shows the highest correlation on longer time-scales with normalized runoff. However, GPCP is discontinued and cannot serve as a near real-time monitoring tool in the future, but serve as a benchmark observational tool. In this study it was also used to bias-correct the reanalysis data. The main conclusions from this study are:

- Drought monitoring in Africa with ERA-Interim is mainly possible outside the ITCZ
- The usefulness of near-real time monitoring tools has to be carefully selected depending on region

4.2 FORECASTING DROUGHTS

System 4 does show skill as a forecasting tool in most basins, and in no basin is it performing worse than the climate. However on longer time scales, where a merge with observational datasets are needed, the selection of the best observation dataset can be a problem,

The main conclusions are:

- The system 4 seasonal forecast has predictive skill which is higher than using climatology for most regions
- In regions where no reliable near real-time data is available it is better to use just the seasonal forecast for prediction of droughts.

Future research has to investigate the impact of the framework introduced in this paper on hydrology and agriculture (see DEWFORA report D4.8, D4.11), It is further necessary to investigate the results in more detail in individual case studies (e.g. the Blue Nile, see future

DEWFORA D4.4), The role, quality and skill of other drought indicators has to be established.

5. REFERENCES

Agustí-Panareda, A., G. Balsamo, and A. Beljaars, 2010: Impact of improved soil moisture on the ECMWF precipitation forecast in West Africa, *Geophys. Res. Lett.*, **37**(L20808), doi: 10.1029/2010GL044748

Balsamo, G., S. Boussetta, E. Dutra, A. Beljaars, P. Viterbo, and B. Van den Hurk, 2011: Evolution of land surface processes in the IFS, *ECMWF Newsletter*, **127**, 17-22.

Berrisford, P., D. Dee, M. Fielding, M. Fuentes, P. Kallberg, S. Kobayashi, and S. M. Uppala, 2009: The ERA-Interim Archive, *ERA Report Series*, **No. 1**, ECMWF, Shinfield Park, Reading, UK.

Dai, A., and K. E. Trenberth, 2002: Estimates of Freshwater Discharge from Continents: Latitudinal and Seasonal Variations, *J. Hydrometeor.*, **3**(6), 660-687, doi: 10.1175/1525-7541(2002)003<0660:eofdfc>2.0.co;2.

Dee, D. P., and Coauthors, 2011: The ERA-Interim reanalysis: configuration and performance of the data assimilation system, *Quart. J. Roy. Meteor. Soc.*, **137**(656), 553-597, doi: 10.1002/qj.828.

Greenwood, J. A., and D. Durand, 1960: Aids for Fitting the Gamma Distribution by Maximum Likelihood, *Technometrics*, **2**(1), 55-56.

Hersbach, H., 2000: Decomposition of the Continuous Ranked Probability Score for Ensemble Prediction Systems, *Weather and Forecasting*, **15**(5), 559-570, doi: 10.1175/1520-0434(2000)015<0559:dotcrp>2.0.co;2.

Huffman, G. J., R. F. Adler, D. T. Bolvin, and G. Gu, 2009: Improving the global precipitation record: GPCP Version 2.1, *Geophys. Res. Lett.*, **36**(17), L17808, doi: 10.1029/2009gl040000.

Huffman, G. J., D. T. Bolvin, and R. F. Adler, 2011: GPCP Version 2.2 Combined Precipitation Data set., WDC-A, NCDC, Asheville, NC. Data set accessed October 2011 at http://www.ncdc.noaa.gov/oa/wmo/wdcamet-ncdc.html.

Ingram, K. T., M. C. Roncoli, and P. H. Kirshen, 2002: Opportunities and constraints for farmers of west Africa to use seasonal precipitation forecasts with Burkina Faso as a case study, *Agricultural Systems*, **74**(3), 331-349.

Janowiak, J. E., and P. Xie, 1999: CAMS-OPI: A Global Satellite-Rain Gauge Merged Product for Real-Time Precipitation Monitoring Applications, *J. Climate*, **12**(11), 3335-3342, doi: 10.1175/1520-0442(1999)012<3335:coagsr>2.0.co;2.

Jones, J. W., J. W. Hansen, F. S. Royce, and C. D. Messina, 2000: Potential benefits of climate forecasting to agriculture, *Agriculture, Ecosystems & Environment*, **82**(1â€“3), 169-184.

Keyantash, J., and J. A. Dracup, 2002: The quantification of drought: An evaluation of drought indices, *Bull. Amer. Meteor. Soc.*, **83**(8), 1167-1180.

Lamb, P. J., R. P. Timmer, xe, and Mi, 2011: Professional development for providers of seasonal climate prediction, *Climate Research*, **47**(1-2), 57-75, doi: 10.3354/cr00949.

Lloyd-Hughes, B., and M. A. Saunders, 2002: A drought climatology for Europe, *Int. J. Climatol.*, **22**(13), 1571-1592.

Luo, L., E. F. Wood, and M. Pan, 2007: Bayesian merging of multiple climate model forecasts for seasonal hydrological predictions, *J. Geophys. Res.*, **112**(D10), D10102, doi: 10.1029/2006jd007655.

Mckee, T. B., N. J. Doesken, and J. Kleist, 1993: The relationship of drought frequency and duration to time scales. *Eight Conference on Applied Climatology*.

Millner, A., and R. Washington, 2011: What determines perceived value of seasonal climate forecasts? A theoretical analysis, *Global Environmental Change*, **21**(1), 209-218.

Molteni, F., and Coauthors, 2011: The new ECMWF seasonal forecast system (System 4), *ECMWF Tech. Memo.*, **656**, 49 pp.

Prigent, C., F. Papa, F. Aires, W. B. Rossow, and E. Matthews, 2007: Global inundation dynamics inferred from multiple satellite observations, 1993–2000, *J. Geophys. Res.*, **112**(D12), D12107, doi: 10.1029/2006jd007847.

Simmons, A. J., and A. Hollingsworth, 2002: Some aspects of the improvement in skill of numerical weather prediction, *Quart. J. Roy. Meteor. Soc.*, **128**(580), 647-677, doi: 10.1256/003590002321042135.

Svoboda, M., and Coauthors, 2002: The Drought Monitor, *Bull. Amer. Meteor. Soc.*, **83**(8), 1181-1190, doi: 10.1175/1520-0477(2002)083<1181:tdm>2.3.co;2.

Thomson, M. C., and Coauthors, 2006: Malaria early warnings based on seasonal climate forecasts from multi-model ensembles, *Nature*, **439**(7076), 576-579.

Tompkins, A. M., and L. Feudale, 2009: Seasonal Ensemble Predictions of West African Monsoon Precipitation in the ECMWF System 3 with a Focus on the AMMA Special Observing Period in 2006, *Weather and Forecasting*, **25**(2), 768-788, doi: 10.1175/2009waf2222236.1.

Van den Hurk, B., P. Viterbo, A. C. M. Beljaars, and A. K. Betts, 2000: Offline validation of the ERA40 surface scheme, *ECMWF Tech. Memo.*, **295**, 42 pp.

Vicente-Serrano, S., 2006: Differences in spatial patterns of drought on different time scales: An analysis of the Iberian Peninsula, *Water Resources Management*, **20**(1), 37-60.

Vicente-Serrano, S. M., and Coauthors, 2012: Challenges for drought mitigation in Africa: The potential use of geospatial data and drought information systems, *Applied Geography*, **34**(0), 471-486, doi: 10.1016/j.apgeog.2012.02.001.

WMO, 2009, **Press release, December 2009 No 872**.

Wood, A. W., and J. C. Schaake, 2008: Correcting Errors in Streamflow Forecast Ensemble Mean and Spread, *J. Hydrometeor.*, **9**(1), 132-148, doi: 10.1175/2007jhm862.1.

Xie, P., and P. A. Arkin, 1997: Global Precipitation: A 17-Year Monthly Analysis Based on Gauge Observations, Satellite Estimates, and Numerical Model Outputs, *Bull. Amer. Meteor. Soc.*, **78**(11), 2539-2558, doi: 10.1175/1520-0477(1997)078<2539:gpayma>2.0.co;2.

Xie, P., and P. A. Arkin, 1998: Global Monthly Precipitation Estimates from Satellite-Observed Outgoing Longwave Radiation, *J. Climate*, **11**(2), 137-164, doi: 10.1175/1520-0442(1998)011<0137:gmpefs>2.0.co;2.

Yamazaki, D., T. Oki, and S. Kanae, 2009: Deriving a global river network map and its sub-grid topographic characteristics from a fine-resolution flow direction map, *Hydrol. Earth Syst. Sci.*, **13**(11), 2241-2251, doi: 10.5194/hess-13-2241-2009.

Yoon, J.-H., K. Mo, and E. F. Wood, 2012: Dynamic-Model-Based Seasonal Prediction of Meteorological Drought over the Contiguous United States, *J. Hydrometeor.*, **13**(2), 463-482, doi: 10.1175/jhm-d-11-038.1.

6. SUPPLEMENTARY FIGURES

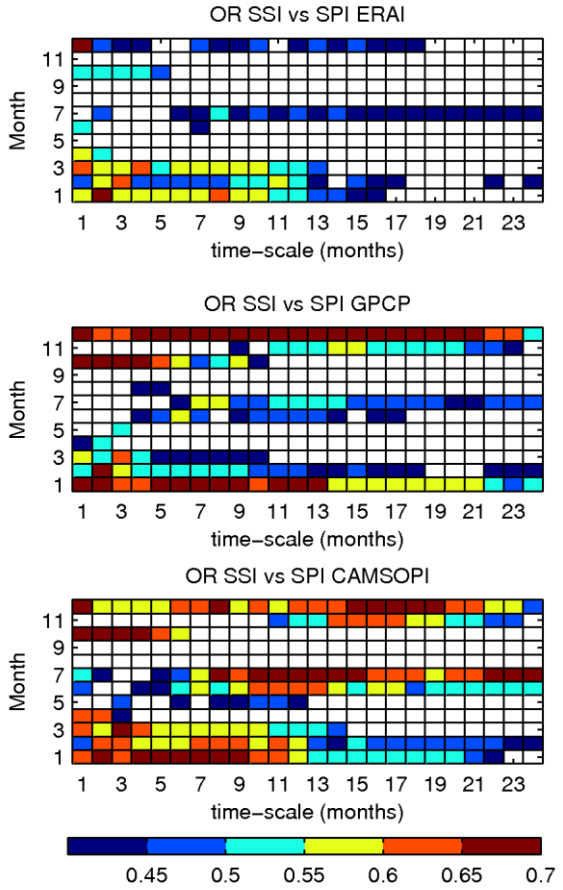

Figure 19. As Figure 12 but for the OR basin. River discharge taken from Dai and Trenberth (2002).

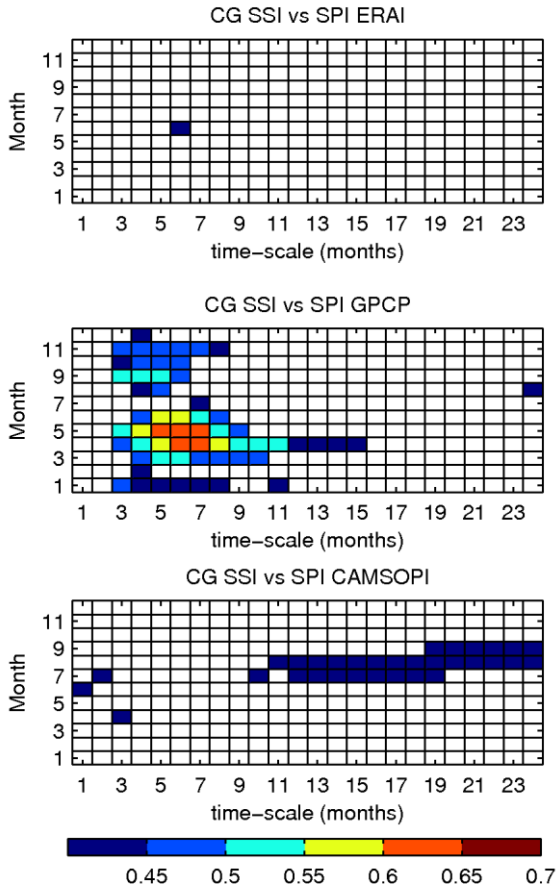

Figure 20. As Figure 12 but for the CG basin. River discharge taken from Dai and Trenberth (2002).

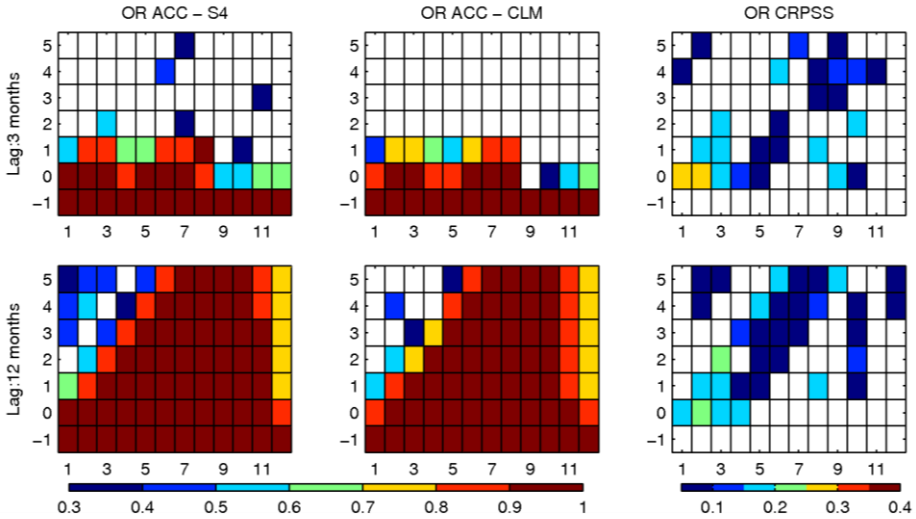

Figure 21. As Figure 16 but for the OR basin

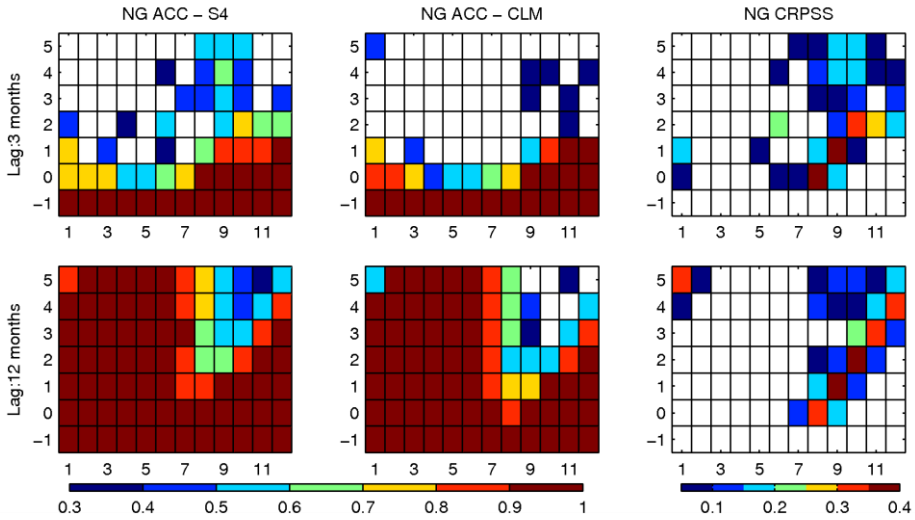

Figure 22. As Figure 16 but for the NG basin

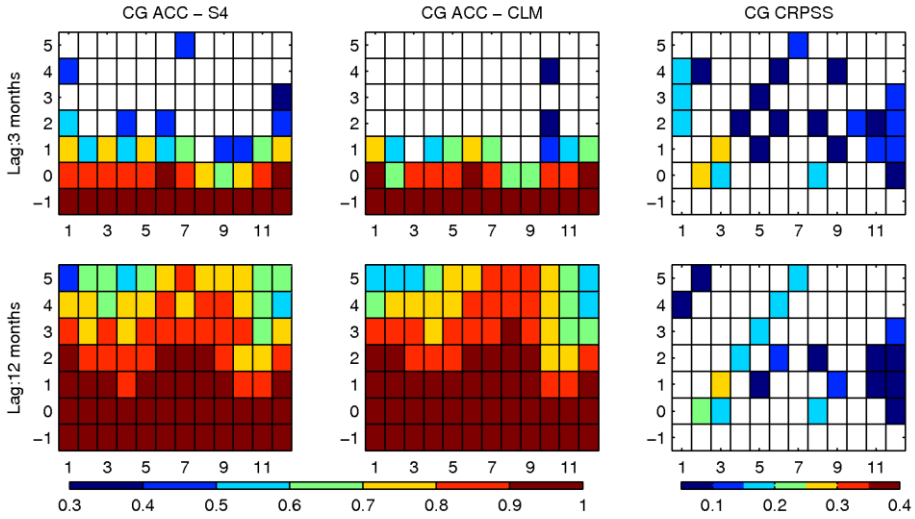

Figure 23. As Figure 16 but for the CG basin

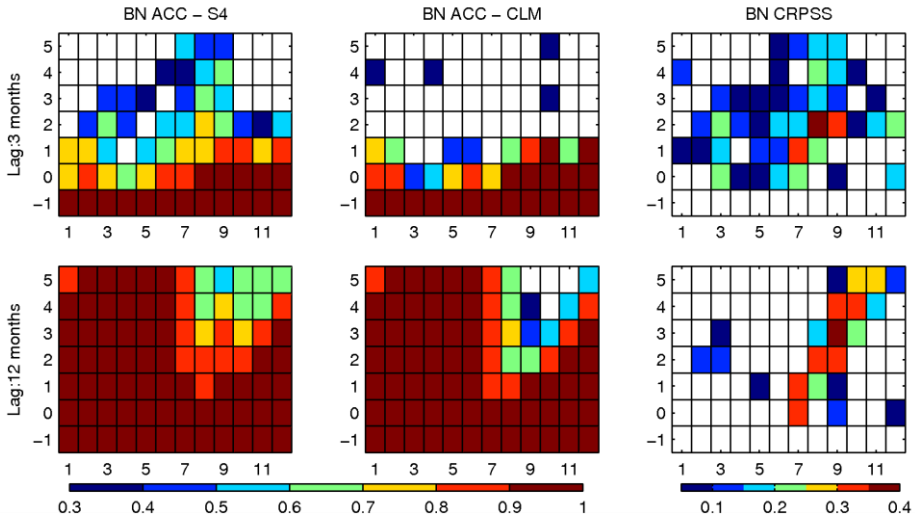

Figure 24. As Figure 16 but for the BN basin

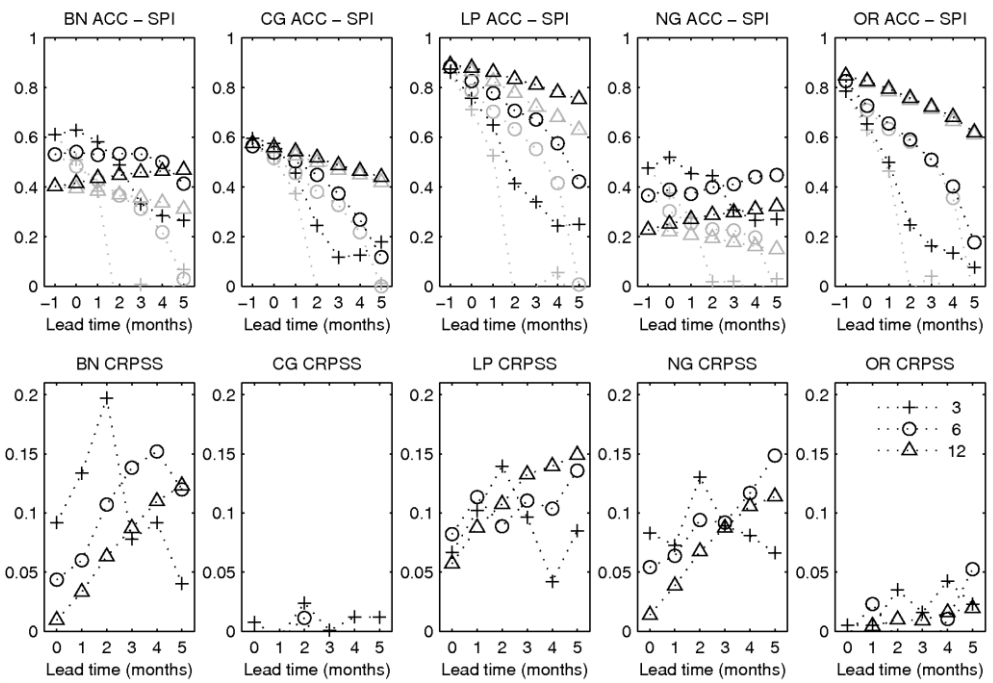

Figure 25. As Figure 15 but using CAMSOPI for monitoring.

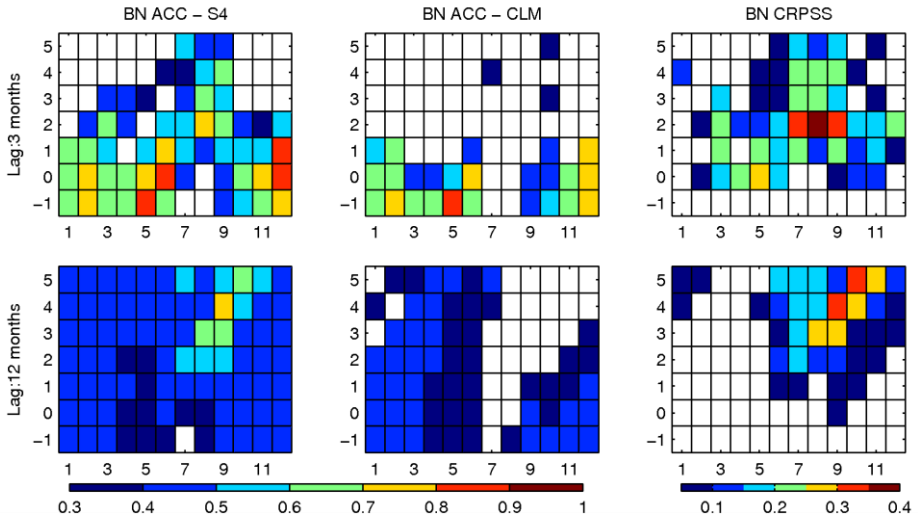

Figure 26. As Figure 16 but for the BN basin using CAMSOPI as monitoring.

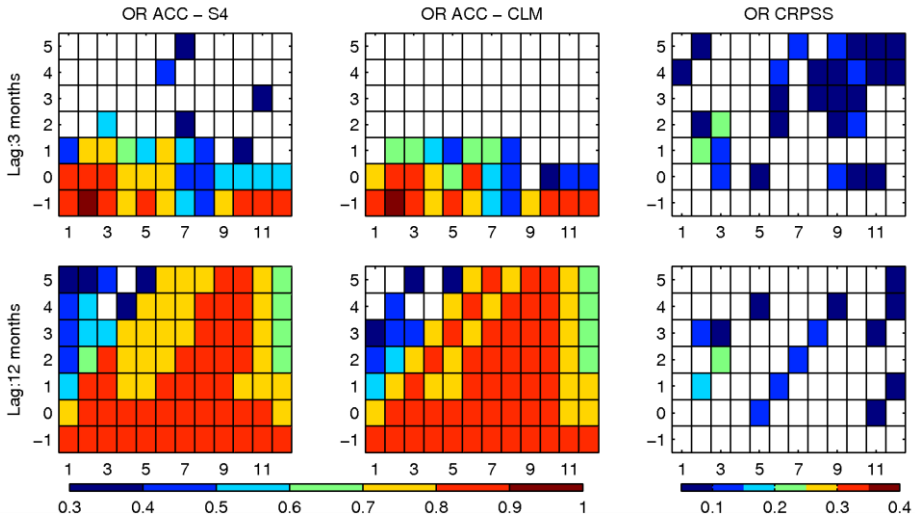

Figure 27. As Figure 16 but for the OR basin using CAMSOPI as monitoring.

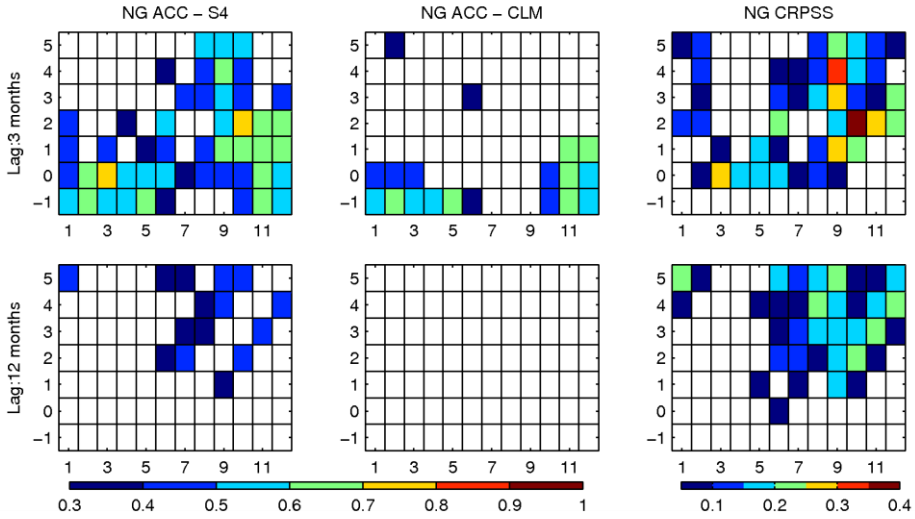

Figure 28. As Figure 16 but for the NG basin using CAMSOPI as monitoring.

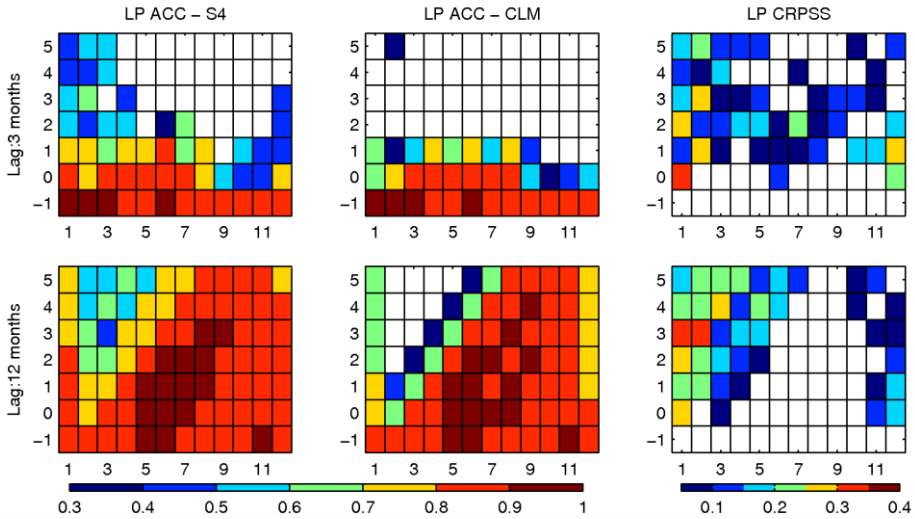

Figure 29. As Figure 16 but for the LP basin using CAMSOPI as monitoring.

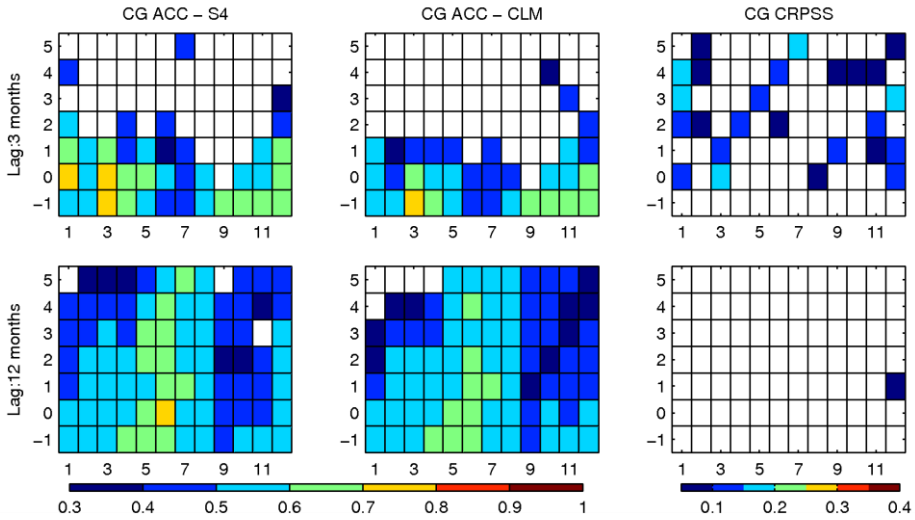

Figure 30. As Figure 16 but for the CG basin using CAMSOPI as monitoring.

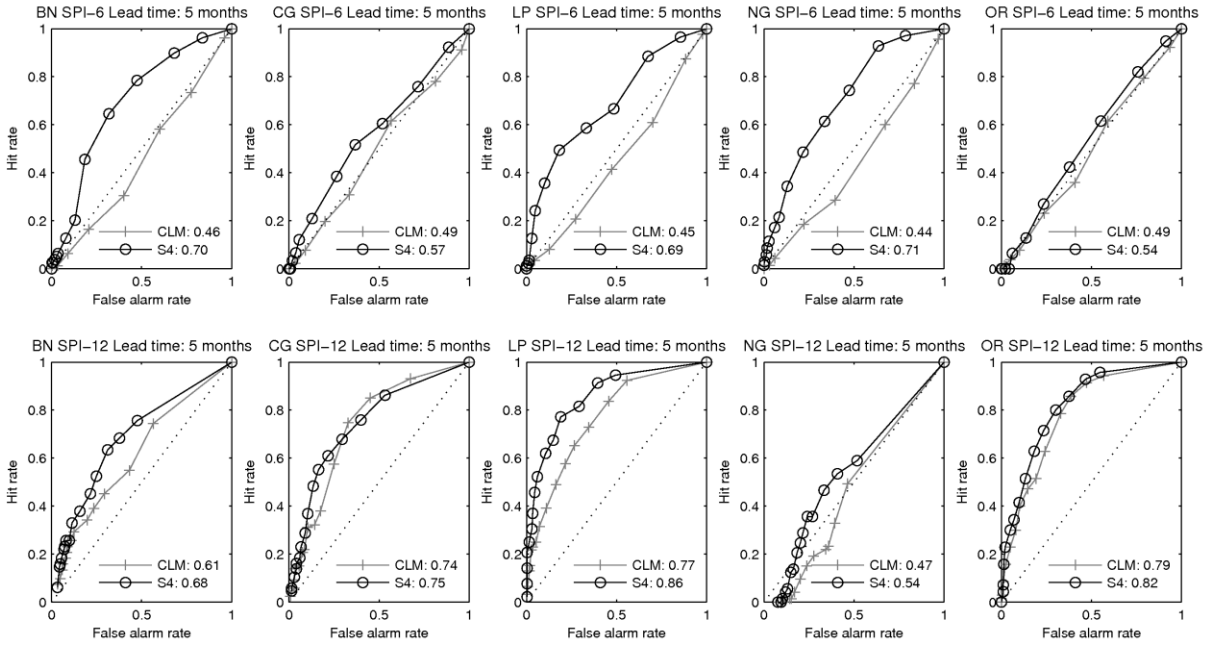

Figure 31. As Figure 17 but using CAMSOPI for monitoring. Note that the top panels are the same as in Figure 17.